



HAL
open science

Spatially Resolved Localization of Lanthanum and Cerium in the Rare Earth Element Hyperaccumulator Fern *Dicranopteris linearis* from China

Wen-Shen Liu, Antony van Der Ent, Peter Erskine, Jean Louis Morel, Guillaume Echevarria, Emmanuelle Montargès-Pelletier, Kathryn Spiers, Rong-Liang Qiu, Ye-Tao Tang

► To cite this version:

Wen-Shen Liu, Antony van Der Ent, Peter Erskine, Jean Louis Morel, Guillaume Echevarria, et al.. Spatially Resolved Localization of Lanthanum and Cerium in the Rare Earth Element Hyperaccumulator Fern *Dicranopteris linearis* from China. *Environmental Science and Technology*, 2020, 54 (4), pp.2287-2294. 10.1021/acs.est.9b05728 . hal-02615658

HAL Id: hal-02615658

<https://hal.science/hal-02615658>

Submitted on 16 Nov 2020

HAL is a multi-disciplinary open access archive for the deposit and dissemination of scientific research documents, whether they are published or not. The documents may come from teaching and research institutions in France or abroad, or from public or private research centers.

L'archive ouverte pluridisciplinaire **HAL**, est destinée au dépôt et à la diffusion de documents scientifiques de niveau recherche, publiés ou non, émanant des établissements d'enseignement et de recherche français ou étrangers, des laboratoires publics ou privés.

1 **Spatially-resolved localization of Rare Earth Elements (REEs)**
2 **in the fern *Dicranopteris linearis* from China**

3
4 Wen-Shen Liu^{1,2,3}, Antony van der Ent^{4,5}, Peter D. Erskine⁴, Jean Louis Morel⁵,
5 Guillaume Echevarria^{4,5}, Emmanuelle Montargès-Pelletier⁶, Kathryn M. Spiers⁷,
6 Rong-Liang Qiu^{1,2,3}, Ye-Tao Tang^{1,2,3,*}

7
8 ¹School of Environmental Science and Engineering, Sun Yat-sen University, Guangzhou 510275, China.

9
10 ²Guangdong Provincial Key Laboratory of Environmental Pollution Control and Remediation Technology
11 (Sun Yat-sen University), Guangzhou 510275, China.

12
13 ³Guangdong Provincial Engineering Research Center for Heavy Metal Contaminated Soil Remediation, Sun
14 Yat-sen University, Guangzhou 510275, China.

15
16 ⁴Centre for Mined Land Rehabilitation, Sustainable Minerals Institute, The University of Queensland, St
17 Lucia, Queensland 4072, Australia.

18
19 ⁵Université de Lorraine, INRA, Laboratoire Sols et Environnement, Nancy 54000, France.

20
21 ⁶Laboratoire Interdisciplinaire des Environnements Continentaux, CNRS - Université de Lorraine,
22 Vandoeuvre-lès-Nancy F-54501, France.

23
24 ⁷Photon Science, Deutsches Elektronen-Synchrotron DESY, Hamburg 22607, Germany.

25
26 ***Corresponding author: Ye-Tao Tang**

28 **Address:** School of Environmental Science and Engineering, Sun Yat-sen University, Guangzhou
29 510275, China
30 **Telephone:** +86 020-84113454
31 **Fax:** +86 020-84110508
32 **E-mail:** eestyty@mail.sysu.edu.cn (Y.T. Tang)

33 **Summary**

34

35 • The fern *Dicranopteris linearis* (Gleicheniaceae) from China is a hyperaccumulator of Rare
36 Earth Elements (REEs), but little is known about its ecophysiology in relation to REEs. This
37 study aimed to clarify tissue-tissue and organ-level distribution of REEs via synchrotron-
38 based X-ray fluorescence microscopy (XFM).

39

40 • The results show that La + Ce are mainly co-localized with Mn in the pinnae and pinnules,
41 with the highest concentrations in necrotic tissues.

42

43 • In the cross-sections of the pinnules, midveins, petioles and stolons La + Ce and Mn are
44 enriched in the epidermis, vascular bundles, and pericycle (midvein). In these tissues, Mn is
45 localised mainly in the cortex and mesophyll compared to La + Ce in these cross-sections.

46

47 • We hypothesize that REEs transpiration flow in the veins is initially restricted by the
48 pericycle between vascular bundle and cortex, whilst excess REEs are transported by
49 evaporation and co-compartmentalized with Mn in the necrotic tissues and epidermis in an
50 immobile form, possibly an Si-coprecipitate.

51

52 **Key words:** X-ray fluorescence microscopy; compartmentalization; necrosis; vein; manganese;
53 silicon.

54

55 **Introduction**

56

57 Rare earth elements (REEs), which include 14 lanthanides and yttrium (Y), have a range of
58 applications in modern technologies, such as high-strength magnets, electric vehicles and medical
59 devices, and increasing demand for these technologies has resulted in a growing need for REEs
60 (Binnemans *et al.*, 2013). Consequently, mining activities and a subsequent release of wastes into the
61 environment, may pose a threat to agricultural crops and human health (Migaszewski & Galuszka,
62 2015).

63

64 Some REEs can be beneficial to plants at low concentrations (Redling, 2006), yet can be toxic to
65 plants at higher concentrations (Thomas *et al.*, 2014; Wang *et al.*, 2014). However,
66 hyperaccumulator plants are able to accumulate and tolerate high concentrations of potentially toxic
67 elements in their living shoots (Baker & Brooks, 1989; Reeves, 2003; van der Ent *et al.*, 2013). Thus
68 far ~700 plant species have been reported globally to hyperaccumulate a large variety of metals and
69 metalloids (Reeves *et al.*, 2017 & 2018), but only 22 plant species are currently recognized as REEs
70 (hyper)accumulators (Liu *et al.*, 2018). The threshold concentration for REEs hyperaccumulation is
71 set at 1000 mg kg⁻¹ in the dry biomass of the aerial parts (Wei *et al.*, 2006). This criterion is the same
72 as used for other trace metals (such as Ni) and metalloids (As), which are typically two or three
73 orders of magnitude higher than concentrations present in 'normal' plants (van der Ent *et al.*, 2013).
74 Moreover, the bioaccumulation factor (BF), which is the quotient of REE concentration in shoots to
75 that in soil, is typically >1 in hyperaccumulator plants; which is indicative of a high ability of soil-to-
76 plant metal(loid) transfer (van der Ent *et al.*, 2013).

77

78 Hyperaccumulator plants potentially offer an environmentally-friendly and cost-effective option for
79 phytoremediation of REE polluted soils and recovery of REEs from low-grade ores and mining
80 wastes (van der Ent *et al.*, 2015; Liu *et al.*, 2018). *Dicranopteris linearis* collected from ion-
81 adsorption REE mine tailings in Ganzhou, Jiangxi Province, can yield 10–15 t of dry biomass per ha
82 per year containing 0.2 wt% REEs, yielding 20 to 30 kg REEs ha⁻¹ (unpublished data). Knowledge

83 on the ecophysiology of REE hyperaccumulator plants is important to better understand the
84 mechanisms for uptake, translocation and sequestration of REEs into living shoots. To date, most
85 studies have focused on the uptake of Ni, zinc (Zn), cadmium (Cd) and arsenic (As) in various
86 hyperaccumulator plant models (Hokura *et al.*, 2006; Tappero *et al.*, 2007; Vogel-Mikuš *et al.*,
87 2008; Tian *et al.*, 2009; Hu *et al.*, 2015), while much less is known about the ecophysiology of REE
88 hyperaccumulator plants (Li *et al.*, 2018).

89

90 Elucidating the spatial distribution of metal(loid)s and their associations with other elements is key to
91 understanding the mechanisms of tolerance in hyperaccumulator plants (Zhao *et al.*, 2014; van der
92 Ent *et al.*, 2018). Over the past decades, elemental distribution in tissues, cells and organelles of a
93 selection of hyperaccumulator plants have been studied extensively (*e.g.* van der Ent *et al.*, 2018).
94 Excess metal(loid)s are typically concentrated in bio-inactive tissues of the leaves to minimize the
95 damage to biological activities (*e.g.* Zhao *et al.*, 2014). This includes Ni localised in foliar epidermal
96 layers, vascular tissues and basal parts of trichomes of *Alyssum murale* (Tappero *et al.*, 2007), As in
97 the venules and the edges of the pinnae of *Pteris vittata* (Hokura *et al.*, 2006), Zn in the vascular and
98 epidermal tissues of *Sedum alfredii* and *Sedum plumbizincicola* (Tian *et al.*, 2009; Hu *et al.*, 2015),
99 and selenium (Se) in the tips and leaf edge of *Astragalus bisulcatus* and *Stanleya pinnata* (Freeman
100 *et al.*, 2006). Meanwhile, vacuole compartmentalization is thought to be an indispensable component
101 of metal(loid)s detoxification in leaves (Sharma *et al.*, 2016). The vascular system clearly has a
102 critical role in transporting metal(loid)s through xylem and phloem loading and unloading (Tappero
103 *et al.*, 2007; Kitajima *et al.*, 2008; Tian *et al.*, 2009). In the hyperaccumulator *Iberis intermedia*,
104 thallium (Tl) is distributed in the vascular bundles of the leaves (Scheckel *et al.*, 2007), whereas in
105 *Phyllanthus balgooyi* the phloem sap is extremely enriched in Ni (van der Ent and Mulligan, 2015)
106 and in *Pycnanandra acuminata* the latex is the main storage for Ni (Jaffré *et al.*, 1976).

107

108 Except for cerium (Ce) (+3 and +4 valences) and europium (Eu) (+2 and +3 valences), the REEs are
109 a group of trivalent (+3) elements which show biochemical behavior that differs from other metals
110 *e.g.* higher affinity to O-containing ligands but lower affinity to S-/N-containing ligands than Zn, Ni,

111 Cd, *etc.* (Nieboer & Richardson, 1980). Thus, REEs in (hyper)accumulators may have distinct uptake
112 and transport strategies yet to be fully understood.

113

114 *Dicranopteris linearis* (Gleicheniaceae) is a native pioneer fern common throughout the Old World
115 (sub)tropics and Oceania (USDA, 2018). This species can grow in acidic (pH 4–5) and poor soils,
116 and exhibits high phosphorus use efficiency (Russell *et al.*, 1998; Chen *et al.*, 2016a). Moreover, *D.*
117 *linearis* often forms patches under an open canopy and dominates the understory of many plant
118 communities in Southern China (*e.g.* *Pinus massoniana*, *Cunninghamia lanceolata*, *Eucalyptus*
119 *robusta*) (Fig. 1). This plant has a crucial role in the ecosystem, retaining nutrients and organic
120 matter (Cohen *et al.*, 1995); sustaining soil microclimates (Zhao *et al.*, 2012); facilitating growth of
121 *Eucalyptus* trees (Wan *et al.*, 2014); and controlling REE migration and gully erosion (Chen *et al.*,
122 2016b). To date, only the *D. linearis* accessions from Southern China have been recognized as a
123 REEs hyperaccumulator (Wei *et al.*, 2001 & 2005; Shan *et al.*, 2003). Field surveys confirm that *D.*
124 *linearis* can accumulate up to 1240–1760 mg kg⁻¹ REEs in the aboveground parts when growing on
125 (ion-adsorption) REE mine tailings (Table S1). *Dicranopteris linearis* thus may be used for
126 phytoremediation and phytomining at ion-adsorption REE mine tailings in Southern China, which
127 can contain 409–1035 mg kg⁻¹ REEs (Chao *et al.*, 2016), and occupy an area of more than 100 km²
128 (Liu *et al.*, 2015). Most of the REEs are accumulated in the cell walls in the pinnae of *D. linearis*, as
129 shown by differential extractions; although some of the REEs are also accumulated within the
130 protoplast, such as the organelles and cytosol, vacuoles and cell membranes (Wei *et al.*, 2005). Light
131 REEs (LREEs, *i.e.* La, Ce, Pr and Nd) deposits have been reported from the cell wall, intercellular
132 space, plasmalemma, vesicles, and vacuoles of the root endodermis and stele cells of the adventitious
133 root by scanning electron microscopy with energy-dispersive spectroscopy (SEM-EDS) (Shan *et al.*,
134 2003). Other studies reported that chlorophyll La and chlorophyll Ce (*i.e.* La and Ce bound to
135 chlorophyll) formed in the pinnae of *D. linearis* (Zhao *et al.*, 1999; Wei *et al.*, 2005), and the
136 chlorophyll REE can partly replace chlorophyll Mg (Wei *et al.*, 2004). Moreover, binding to proteins
137 is likely one of the mechanisms against physiological toxicity of REEs in *D. linearis* pinnae (Wang
138 *et al.*, 2003). Overall, the different techniques and samples preparations used to unravel those

139 different observations may be responsible for some artefacts. The high concentration of histidine
140 reported in the pinnae of this plant (Shan *et al.*, 2003) may result from various physiological
141 activities and its presence is not sufficient to prove or demonstrate the chemical status of REEs, *i.e.*
142 histidine complexes of REEs. The investigation of REE distribution and speciation at a
143 submicrometric scale might provide key information about the mechanisms driving the uptake and
144 storage of those elements by identifying the analogies and co-distributions with other elements,
145 including nutrients.

146

147 Synchrotron-based X-ray fluorescence microscopy (XFM) is a non-destructive method that has been
148 successfully used to study the *in-situ* distribution of trace elements in hyperaccumulator plants (for
149 recent reviews see Lombi & Susini, 2009; van der Ent *et al.*, 2018; Kopittke *et al.*, 2018). The aim of
150 this study was to better understand the ecophysiological mechanisms that enable tolerance to REEs
151 in this fern. To that end, XFM elemental images of the sum of two light REEs (referred to as La + Ce
152 and being the sum of La and Ce), of K, Ca and Mn in the tissues and cells of *D. linearis* frond were
153 acquired.

154

155 **Materials and methods**

156

157 **Collection of plant tissues**

158 Live samples of *D. linearis* grown on the ion-adsorption REE mine tailings of Ganzhou, Jiangxi
159 Province, China (24° 57' N, 115° 05' E), and the corresponding soil material were collected. The
160 plants were transplanted in pots containing soil material and placed in a greenhouse, Sun Yat-sen
161 University, Guangzhou, China. Three mature plants with rhizosphere soil were brought alive to the
162 P06 beamline (PETRA III Synchrotron, DESY, Hamburg, Germany) for the experiments described
163 below. In parallel, four mature live pinna and three standing litter pinna (the dead pinna was still
164 connected to the stolon) samples from a *D. linearis* population on an ion-adsorption REE mine
165 tailing were sampled for bulk chemical analysis (Fig. S1).

166

168 **Chemical analysis of bulk tissue samples**

169 Plant samples were washed with pure water (18 Ω , 25°C), then dried in an oven at 105°C for 2 h and
170 60°C for 72 h. The analysis methods of total concentrations of Al, REEs, Si, and other trace elements
171 (Mn, K, Ca, P) were adapted from Liu *et al.* (2019).

172

173 **X-ray fluorescence microscopy (XFM)**

174 The X-ray fluorescence microscopy (XFM) experiment was undertaken at Beamline P06 at the
175 PETRA III (Deutsches Elektronen-Synchrotron; DESY, Hamburg, Germany), a 6 GeV synchrotron
176 (Boesenberg *et al.*, 2016). The undulator beam was monochromatized with a cryogenically cooled
177 Si(111) channel-cut monochromator to an energy of 12 keV with a flux of 10¹⁰ photon/s. A
178 Kirkpatrick-Baez mirror pair was used to focus the incident beam to 700 × 530 nm (hor × ver). The
179 samples were scanned in fly-scan mode, with the resultant sample X-ray signal detected using the
180 Maia 384C detector system, operated in backscatter geometry (Kirkham *et al.*, 2010; Ryan *et al.*,
181 2010 & 2014; Siddons *et al.*, 2014). Typically, a quick ‘survey scan’ was first conducted to allow
182 for the selection of the appropriate portion of the sample. For the survey scan, the resolution was 50–
183 100 μ m with a dwell of 1–2 ms and generally took ca. 5 min to complete. After that a ‘detailed scan’
184 was conducted, with a resolution of 2–10 μ m and a dwell time of 8–20 ms. For the whole
185 experiment, the incident energy of 12 keV was used in order that the fluorescence lines of the
186 elements of interest are well below the inelastic and elastic scatter peaks.

187

188 Live/fresh pinnule samples were analysed whole, or as cross-sections which hand cut with a
189 stainless-steel razor blade (‘dry knife’ method); whole or sectioned samples were then mounted
190 between two sheets of 4 μ m Ultralene thin film in a tight sandwich to limit evaporation, and analysed
191 within 10 minutes after excision. The fresh samples mounted between two sheets of Ultralene thin
192 film (4 μ m) were stretched over a 3D-printed frame magnetically attached to the *x-y-z* sample stage
193 at atmospheric temperature (~23°C). X-ray micro-fluorescence was performed using fast scanning to
194 keep the scan time, and hence sample degradation, to a minimum.

195 **Data processing and statistics**

196 The XRF event stream was analysed using the Dynamic Analysis method (Ryan & Jamieson, 1993;
197 Ryan, 2000) as implemented in GeoPIXE (Ryan *et al.*, 1990 & 2005). It was necessary to use a
198 precise matrix file for the spectra fitting to account for X-ray fluorescence absorption of the
199 relatively low energy of the REEs L-lines, and the matrix was based on the stoichiometry of the
200 mean concentrations of major elements (>0.1 wt%) in dried *D. linearis* pinna samples (Table S2).
201 The matrix composition assumed hydration of the fresh samples, and was formulated as
202 $C_7O_{31}H_{59}N_{0.7}S_{0.2}Al_{0.3}Si_{1.5}Ca_{0.2}Mn_{0.1}K_{0.3}$ (on the basis of average concentrations of these elements in
203 bulk samples) with a density of 0.90 g cm^{-3} , considering two layers of Ultralene foil ($4 \mu\text{m}$) and with
204 varying sample thicknesses. Pinnule samples were considered to have uniform thickness. The
205 rhodium coating of the KB mirror focusing optics available for this experiment results in a
206 high-energy cutoff of 23 keV, well below that required to excite the K-lines of the REEs (33.44 keV
207 for La), so therefore the experiment had to rely on exciting the L-lines (ranging from 4.65 keV for La
208 to 7.41 keV for Yb). The L-lines of Al and Si were around 1.5–3 keV, thus could not be detected.
209 Although the K-line of Y could be reached at 14.96 keV, its concentration was too low (mean of 106
210 $\mu\text{g g}^{-1}$ Y in pinna) to be reliably detected. The reported resolution of the Maia 384C detector is 220
211 eV and it is hence unable to distinguish between the numerous L-lines of various the REEs.
212 Moreover, the L-lines of Gd, Eu and Sm are in the range of the K-lines of Mn and thus these
213 elements, at these relative concentrations, are not possible to distinguish reliably using the Maia
214 detector. Consequently, only La and Ce were used to represent the REEs.

215

216 **Results**

217

218 **Bulk elemental concentrations in *Dicranopteris linearis***

219 The bulk pinna concentrations of REEs, Al, Si, Mn, K, Ca, and P are given in Table 1. The
220 concentrations of Al, Si and REEs in live pinnae are around half that of the standing litter pinnae –
221 Al 2850 vs 4850 mg kg^{-1} , Si 14700 vs 33900 mg kg^{-1} and REEs 1900 vs 3500 mg kg^{-1} respectively.

222 Alternatively, the concentrations of Mn, P and K in live pinnae are always higher than the standing
223 litter pinnae – Mn 1480 vs 310 mg kg⁻¹, P 211 vs 129 mg kg⁻¹ and K 3000 vs 268 mg kg⁻¹
224 respectively. The concentration of Ca has no significant difference between the two types of pinnae
225 (Table 1). Among the 15 REEs, the sum of La and Ce accounts for ~50% of the total REEs in the
226 pinnae, without significant differences between live and standing litter pinnae (Table S2).

227

228 **Localization of REEs in pinna and pinnule**

229 The X-ray fluorescence element maps evidenced a distinct mapping for K, Ca, Mn and the summed
230 REEs La + Ce in the tissues of the pinna (Fig. 2; Fig. 3) and the pinnule (Fig. 4; Fig. 5; Fig. S2) of *D.*
231 *linearis*. The most significant enrichment of La + Ce and Mn is in the necrotic tissues, which are by
232 definition the bio-inactive regions of the pinna. The preferential accumulation of REEs in these
233 necrotic spots appear to in all of the tissue areas (pinna tips, margins and blades) of the necrosis.
234 Significant La + Ce and Mn enrichments are also in the midvein, secondary veins, tertiary veins and
235 in the margins of the pinna and its pinnule. The La + Ce and Mn were not strictly restricted within
236 the veins and necrotic tissues; their signals were also visibly and uniformly localized outside the
237 veins and necrotic tissues. Calcium is mainly distributed in the necrotic tissues and blade, but low in
238 the veins. Potassium has a distinctly different distribution in the pinna and pinnule, and is mostly
239 localized in the blade, and absent in the necrotic tissues.

240

241 In order to compare the elements spatial co-occurrences and correlations, tri-color (Ce, Mn and Ca)
242 composites maps and Ce-Mn frequency plots of a pinna and a pinnule are provided in Fig. S3. The
243 results further confirm the co-localization of Ce and Mn both inside and outside the necrotic tissues,
244 with higher concentrations inside the necrotic tissues and lower outside. However, tri-color elemental
245 maps and element association frequency plots also show that Ce and Mn are not totally co-localized,
246 e.g. there are some high Ce areas at the right of the pinnule (Fig. S2), where Mn is relatively low.

247

248

249 **Localization of REEs in pinnule and midvein cross-section**

250 In order to establish the localization of REEs at the cellular level, XFM mapping was performed on
251 cross-sections of midvein and pinnule. The elemental maps revealed that La + Ce and Mn are co-
252 localized in the epidermis (Fig. 6; Fig. 7). The La + Ce and Mn in the upper epidermis are much
253 more concentrated than in the low epidermis. In the midvein cross-section, there is a “ring” shaped
254 peak of La + Ce and Mn between the vascular bundle and the cortex, likely the pericycle. In the
255 pinnule cross-section, the vascular bundle and cortex are difficult to differentiate. However,
256 compared to La + Ce, Mn signals are more prominent in the cortex and mesophyll, while less marked
257 in the vascular bundle. Potassium is low in the cortex, but concentrated in the mesophyll, epidermis
258 and vascular bundle. Calcium is predominantly localized in the mesophyll and epidermis, but low in
259 the vascular bundle and cortex. The subcellular elemental distribution could not be differentiated for
260 any element.

261

262 **Localization of REEs in petiole and stolon cross-section**

263 The elemental XFM maps of the petiole and stolon cross-sections show La + Ce enrichment in the
264 epidermis and vascular bundle, while in the cortex and the pericycle of the petiole cross-section
265 prevailing concentrations are very low (Fig. 8 and Fig. S4). In contrast, in both the petiole and stolon
266 cross-sections, the K, Ca and Mn are similar and mostly concentrated in the epidermis, pericycle and
267 vascular bundle, with distinct localizations in the cortex. Within the vascular bundle of petiole cross-
268 sections, La + Ce, Mn, K and Ca are mainly localized in the protoxylem and metaxylem.

269

270 **Discussion**

271

272 *Dicranopteris linearis* accumulates the highest concentrations of REEs in necrotic tissues, which
273 differs significantly from the behavior of most other metal hyperaccumulators. Potassium is an
274 essential element that plays a critical role in cellular osmotic regulation in the young and fresh leaves,
275 and the absence of K in necrotic tissues suggests that these areas are physiologically inactive. The

276 markedly higher concentrations of REEs, Al and Si in the standing litter pinnae, as compared to the
277 live pinnae further affirms that these elements are rather immobile as opposed to K which is strongly
278 depleted in litter tissues (Fig. S1; Table 1). The concentrations of Mn in the pinna of *D. linearis*
279 (Table 1) are much greater than what is typically toxic in most of the plants (*e.g.* < 200 mg kg⁻¹ in
280 maize) (Shao *et al.*, 2017). Therefore, the necrosis in these tissues is possibly, among other reasons,
281 the result of Mn accumulation, oxidation and localised toxicity within the pinnules, which then
282 induces cell death, necrotic spots, substantially larger necrotic tissue and then finally acts as a “dump
283 site” for REEs. A similar phenomenon has been reported in the leaf of soybean and cowpea in
284 response to Mn toxicity; the toxicity started with Mn pumped under the cuticle via the apoplast, or
285 expelled via hydathodes towards the leaf tip, and then increasing concentrations of Mn leading to Mn
286 oxidation (+2 to +3 and +4 valences) and necrotic lesions, which in turn stimulate more Mn
287 translocation as a result of higher evaporation (Blamey *et al.*, 2018a & 2018b). However, Ce and Mn
288 were not totally co-localized, it is therefore also possible that the necrotic tissues were induced by Ce
289 accumulation and oxidation (+3 to +4 valences). It could be also interpreted as a tolerance
290 mechanism in which some cells are sacrificed and used as a dump, while in the others,
291 photosynthesis and normal activity can continue (Küpper *et al.*, 2007). The underlying mechanisms
292 as to why REEs prefer to compartmentalize into the upper epidermis, margins and veins are not fully
293 understood. Previous studies on hyperaccumulator plants suggest that it may reflect a physiological
294 and/or defense-related response – protection of photosynthetically active tissues such as mesophyll,
295 and defense from predation by herbivores and pathogens (Martens & Boyd, 1994; Cappa & Pilon-
296 Smits, 2014).

297

298 The distinct localization in vascular bundles, while prevailing concentrations are low in the cortex of
299 petiole and midvein, suggests an efficient REE transport system in this plant. The transport of REEs
300 to the pinna probably occurs as mass flow through the vascular tissue, driven by transpiration. In
301 non-accumulating species of beech and oak (Fagaceae), REEs transport within xylem was suggested
302 to be associated with general nutrient flux (Brioschi *et al.*, 2013). However, in the vascular bundles
303 of *D. linearis*, we found both a small area of La + Ce peaks within vascular bundle and a very bright

304 “ring” shaped peak between vascular bundle and cortex (Fig. 7). The significant La + Ce enrichment,
305 with no obvious Ca and Mn enrichment within the vascular bundle of veins, suggests that REEs are
306 translocated to the blade to a lesser extent than Ca and Mn. This might be due to the features of the
307 pericycle tissue where cells are dense, preventing REEs translocation from the xylem into the blade
308 via the intercellular space. It is possible that once the REEs enter into the vascular system of veins
309 (xylem), they are partly fixed by the pericycle, and then transported to the *D. linearis* blades
310 (especially to the epidermis and necrotic tissues) via transpiration flow. In this case, the transport and
311 accumulation of REEs should mainly be passive convection processes. Thus, the distribution of
312 REEs in *D. linearis* pinna could be influenced by various parameters that are associated with the
313 evaporation (*e.g.* biological variety, seasonal and climatic changes) and Mn toxicity (*e.g.* light,
314 pinnule age and height at sampling) (Küpper *et al.*, 2004; Fernando & Lynch, 2015; Bartoli *et al.*,
315 2018). The highest concentrations recorded within the necrotic tissues of pinna may be ascribed to a
316 lack of wax coats at the surface of pinna, and/or the damage of the pericycle tissue or cells between
317 vascular bundle and cortex in the veins, thus leading to a higher evaporation rate. The higher
318 evaporation rate may also lead to higher concentrations of REEs in the upper epidermis, compared to
319 the lower epidermis (Fig. 6; Fig. 7).

320

321 As vacuoles in necrotic tissues of the pinnae disintegrate, compartmentalization and accumulation in
322 these areas indicate that the REEs are likely to be sequestered by cell walls or exist under immobile
323 forms. Many studies found that REEs tend to complex with phosphate and form deposits in the cell
324 walls and more generally in the intercellular space of plant tissues (Ding *et al.*, 2006; Ruíz-Herrera *et al.*,
325 2012). However, the molar ratio of P in *D. linearis* pinnae was much lower than that of REEs
326 (Table 1). Moreover, we found that *D. linearis* also accumulates high concentration of Al and Si
327 (Table 1; Chour *et al.*, 2018). Detoxification of Al and other heavy metals by Si has been observed in
328 many plants (Liang *et al.*, 2007). For example, Al localization coincided with Si distribution in cell
329 walls of the Al hyperaccumulator *Rudgea viburnoides* (Malta *et al.*, 2016). The co-deposition of Si
330 and Cd in the cell walls as a [Si-wall matrix]Cd co-complex inhibited Cd ion uptake by rice cell (Liu
331 *et al.*, 2013). In the Al and Si hyperaccumulator *Faramaea marginata*, Al and Si are thought to be co-

332 deposited as phytolith Al (Britez *et al.*, 2002). Also, silicon may co-deposit with Mn at the apoplast
333 and decrease the oxidation of Mn in cowpea, soybean and sunflower (Blamey *et al.*, 2018a). Rare
334 earth elements are a group of trivalent elements, which exhibit many chemical similarities to Al
335 (Pletnev & Zernov, 2002). Considering the high concentration of REEs, Mn, Al and Si, a co-
336 deposition of REEs, Mn and Al with Si may be involved in the homeostasis of high concentrations of
337 REEs, Mn and Al in *D. linearis*. Therefore, it would be crucial to study the localization of Al and Si
338 in *D. linearis* tissues with other methods to confirm these hypotheses.

339

340 **Author contributions**

341

342 WSL conducted the fieldwork and collected the samples. AvdE, GE, PDE and KMS conducted the
343 synchrotron XFM experiment. KMS, AvdE and EMP performed the XFM data processing and
344 analysis. WSL conducted and bulk elemental analysis. All authors contributed to writing the
345 manuscript.

346

347 **Acknowledgements**

348

349 This work was financially supported by the National Natural Science Foundation of China
350 (41771343), and the 111 Project (B18060). This work is a contribution of the joint lab ECOLAND,
351 established between Sun Yat-sen University, University of Lorraine and INRA. We acknowledge
352 DESY (Hamburg, Germany), a member of the Helmholtz Association HGF, for the provision of
353 experimental facilities. Parts of this research were carried out at PETRA III and we would like to
354 thank Dr. Jan Garrevoet and Dr. Gerald Falkenberg for assistance in using beamline P06. The
355 research leading to this result has been supported by the project CALIPSOplus under the Grant
356 Agreement 730872 from the EU Framework Programme for Research and Innovation HORIZON
357 2020. The French National Research Agency through the national “Investissements d’avenir”
358 program (ANR-10-LABX-21, LABEX RESSOURCES21) and through the ANR-14-CE04-0005
359 Project “Agromine” is acknowledged for funding support.

360

361

362 **References**

363

364 **Baker AJM, Brooks RR. 1989.** Terrestrial higher plants which hyper accumulate metallic elements.
365 *Biorecovery* **1**: 81–126.

366 **Bartoli F, Royer M, Coinchelin D, Thiec DL, Rose C, Robin C, Echevarria G. 2018.** Multiscale
367 and age-dependent leaf nickel in the Ni-hyperaccumulator *Leptoplax emarginata*. *Ecological*
368 *Research* **33**: 1–14.

369 **Binnemans K, Jones PT, Blanpain B, Gerven TV, Yang Y, Walton A, Buchert M. 2013.**
370 Recycling of rare earths: a critical review. *Journal of Cleaner Production* **51**: 1–22.

371 (1) **Blamey** *Plant Soil*. **2019**, *437*, 427–437.

372 (2) Boesenberg, U.; Ryan, C. G.; Kirkham, R.; Siddons, D. P.; Alfeld, M.; Garrevoet, J.; Núñez, T.;
373 Claussen, T.; Kracht, T.; Falkenberg, G. Fast X-ray microfluorescence imaging with
374 submicrometer-resolution integrating a Maia detector at beamline P06 at PETRA III. *J.*
375 *Synchrotron Radiat.* **2016**, *23*, 1550–1560.

376 Kirkham, R.; Dunn, P. A.; Kuczewski, A. J.; Siddons, D. P.; Dodanwela, R.; Moorhead, G. F.; Ryan
377 C. G.; de Geronimo, G.; Beuttenmuller, R.; Pinelli, D.; Pfeffer, M.; Davey, P.; Jensen, M.;
378 Paterson, D. J.; de Jonge, M. D.; Howard, D. L.; Kusel, M.; McKinlay, J **FPC, McKenna BA,**
379 **Li C, Cheng MM, Tang CX, Jiang HB, Howard DL, Paterson DJ, Kappen P, Wang P,**
380 **Menzies NW, Kopittke PM. 2018a.** Manganese distribution and speciation help to explain the
381 effects of silicate and phosphate on manganese toxicity in four crop species. *New Phytologist*
382 **217**: 1146–1160.

383 **Blamey FPC, Paterson DJ, Walsh A, Afshar N, McKenna BA, Cheng MM, Tang CX, Horst**
384 **WJ, Menzies NW, Kopittke PM. 2018b.** Time-resolved X-ray fluorescence analysis of
385 element distribution and concentration in living plants: An example using manganese toxicity
386 in cowpea leaves. *Environmental and Experimental Botany* **156**: 151–160.

- 387 **Boesenberg U, Ryan CG, Kirkham R, Siddons DP, Alfeld M, Garrevoet J, Núñez T, Claussen**
388 **T, Kracht T, Falkenberg G. 2016.** Fast X-ray microfluorescence imaging with
389 submicrometer-resolution integrating a Maia detector at beamline P06 at PETRA III. *Journal of*
390 *Synchrotron Radiation* **23**: 1550–1560.
- 391 **Brioschi L, Steinmann M, Lucot E, Pierret MC, Stille P, Prunier J, Badot PM. 2013.** Transfer
392 of rare earth elements (REE) from natural soil to plant systems: implications for the
393 environmental availability of anthropogenic REE. *Plant and Soil* **366**: 143–163.
- 394 **Britez RM, Watanabe T, Jansen S, Reissmann CB, Osaki M. 2002.** The relationship between
395 aluminium and silicon accumulation in leaves of *Faramea marginata* (Rubiaceae). *New*
396 *Phytologist* **156**: 437–444.
- 397 **Cappa JJ, Pilon-Smits EA. 2014.** Evolutionary aspects of elemental hyperaccumulation. *Planta* **239**:
398 267–275.
- 399 **Chao YQ, Liu WS, Chen YM, Chen WH, Zhao LH, Ding QB, Wang SZ, Tang YT, Zhang T,**
400 **Qiu RL. 2016.** Structure, variation, and co-occurrence of soil microbial communities in
401 abandoned sites of a rare earth elements mine. *Environmental Science & Technology* **50**:
402 11481–11490.
- 403 **Chen ZQ, Chen ZB, Yan XY, Bai LY. 2016a.** Stoichiometric mechanisms of *Dicranopteris*
404 *dichotoma*, growth and resistance to nutrient limitation in the Zhuxi watershed in the red soil
405 hilly region of China. *Plant and Soil* **398**: 367–379.
- 406 **Chen ZQ, Chen ZB, Bai LY. 2016b.** Rare earth element migration in gullies with different
407 *Dicranopteris dichotoma* covers in the Huangnikeng gully group, Changting county, Southeast
408 China. *Chemosphere* **164**: 443–450.
- 409 **Chour Z, Laubie B, Morel JL, Tang YT, Qiu RL, Simonnot MO, Muhr L. 2018.** Recovery of
410 rare earth elements from *Dicranopteris dichotoma* by an enhanced ion exchange leaching
411 process. *Chemical Engineering and Processing* **130**: 208–213.

- 412 **Cohen AL, Singhakumara BMP, Ashton PMS. 1995.** Releasing rain forest succession: a case
413 study in the *Dicranopteris linearis* fernlands of Sri Lanka. *Restoration Ecology* **3**: 261–270.
- 414 **Ding SM, Liang T, Zhang CS, Huang ZC, Xie YN, Chen TB. 2006.** Fractionation mechanisms of
415 rare earth elements (REEs) in hydroponic wheat: an application for metal accumulation by
416 plants. *Environmental Science & Technology* **40**: 2686–2691.
- 417 **Fernando DR, Lynch JP. 2015.** Manganese phytotoxicity: new light on an old problem. *Annals of*
418 *Botany* **116**: 313–319.
- 419 **Freeman JL, Zhang LH, Marcus MA, Fakra S, Mcgrath SP, Pilon-Smits EAH. 2006.** Spatial
420 imaging, speciation, and quantification of selenium in the hyperaccumulator plants *Astragalus*
421 *bisulcatus* and *Stanleya pinnata*. *Plant Physiology* **142**: 124–134.
- 422 **Hokura A, Omuma R, Terada Y, Kitajima N, Abe T, Saito H, Yoshida S, Nakai I. 2006.**
423 Arsenic distribution and speciation in an arsenic hyperaccumulator fern by x-ray spectrometry
424 utilizing a synchrotron radiation source. *Journal of Analytical Atomic Spectrometry* **21**: 321–
425 328.
- 426 **Hu PJ, Wang YD, Przybyłowicz WJ, Li Z, Barnabas A, Wu LH, Mesjasz-Przybyłowicz J.**
427 **2015.** Elemental distribution by cryo-micro-PIXE in the zinc and cadmium hyperaccumulator
428 *Sedum plumbizincicola* grown naturally. *Plant and Soil* **388**: 267–282.
- 429 **Jaffré T, Brooks RR, Lee J, Reeves RD. 1976.** *Sebertia acuminata*: a hyperaccumulator of nickel
430 from New Caledonia. *Science* **193**: 579–580.
- 431 **Kirkham R, Dunn PA, Kuczewski AJ, Siddons DP, Dodanwela R, Moorhead GF, Ryan CG, de**
432 **Geronimo G, Beuttenmuller R, Pinelli D, Pfeffer M, Davey P, Jensen M, Paterson DJ, de**
433 **Jonge MD, Howard DL, Kusel M, McKinlay J. 2010.** The Maia spectroscopy detector
434 system: engineering for integrated pulse capture, low - latency scanning and real - time
435 processing. *AIP Conference Proceedings* **1234**: 240–243.

- 436 **Kitajima N, Kashiwabara T, Fukuda N, Endo S, Hokura A, Terada Y, Nakai I. 2008.**
437 Observation of arsenic transfer in leaf tissue of hyperaccumulator fern by utilizing synchrotron
438 radiation micro-XRF imaging. *Chemistry Letters* **37**: 32–33.
- 439 **Kopittke PM, Punshon T, de Jonge MD, Paterson DJ, Tappero RV, Ryan CG, Wang P,**
440 **Blamey FPC, McKenna BA, van der Ent A, Lombi E. 2018.** Synchrotron-based X-ray
441 fluorescence microscopy as a technique for imaging of elements in plants. *Plant Physiology*
442 **178**: 507–523.
- 443 **Küpper H, Mijovilovich A, Meyerklaucke W, Kroneck PMH. 2004.** Tissue- and age-dependent
444 differences in the complexation of cadmium and zinc in the cadmium/zinc hyperaccumulator
445 *Thlaspi caerulescens* (Ganges ecotype) revealed by x-ray absorption spectroscopy. *New*
446 *Phytologist* **134**: 748–757.
- 447 **Küpper H, Parameswaran A, Leitenmaier B, Trtílek M, Šetlík I. 2007.** Cadmium - induced
448 inhibition of photosynthesis and long - term acclimation to cadmium stress in the
449 hyperaccumulator *Thlaspi caerulescens*. *New Phytologist* **175**: 655–674.
- 450 **Li JT, Gurajala HK, Wu LH, van der Ent A, Qiu RL, Baker AJ, Tang YT, Yang XE, Shu WS.**
451 **2018.** Hyperaccumulator plants from China: A synthesis of the current state of knowledge.
452 *Environmental Science & Technology* **52**: 11980–11994.
- 453 **Liang Y, Sun W, Zhu YG, Christie P. 2007.** Mechanisms of silicon-mediated alleviation of abiotic
454 stresses in higher plants: a review. *Environmental Pollution* **147**: 422–428.
- 455 **Liu C, Yuan M, Liu WS, Guo MN, Huot H, Tang YT, Laubie B, Simonnot MO, Morel JL, Qiu**
456 **RL. 2018.** Agromining: farming for metals. In Element case studies: rare earth elements; van
457 der Ent A, Echevarria G, Baker AJM, Morel JL, eds, *Mineral Resource Reviews series, Cham:*
458 *Springer International Publishing* pp. 297–308.
- 459 **Liu J, Ma J, He CW, Li XL, Zhang WJ, Xu FS, Lin YJ, Wang LJ. 2013.** Inhibition of cadmium
460 ion uptake in rice (*Oryza sativa*) cells by a wall-bound form of silicon. *New Phytologist* **200**:
461 691–699.

- 462 **Liu WS, Liu C, Wang ZW, Teng WK, Tang YT, Qiu RL. 2015.** Limiting factors for restoration of
463 dumping sites of ion-adsorption rare earth tailing. *Acta Ecologica Sinica* **52**: 879–887.
- 464 **Liu WS, Zheng HX, Guo MN, Liu C, Huot H, Morel JL, van der Ent A, Tang YT, Qiu RL.**
465 **2019.** Co-deposition of silicon with rare earth elements (REEs) and aluminium in the fern
466 *Dicranopteris linearis* from China. *Plant and Soil* **437**: 427–437.
- 467 **Lombi E, Susini J. 2009.** Synchrotron-based techniques for plant and soil science: opportunities,
468 challenges and future perspectives. *Plant and Soil* **320**: 1–35.
- 469 **Malta PG, Arcanjo-Silva S, Ribeiro C, Campos NV, Azevedo AA. 2016.** *Rudgea viburnoides*
470 (Rubiaceae) overcomes the low soil fertility of the Brazilian Cerrado and hyperaccumulates
471 aluminum in cell walls and chloroplasts. *Plant and Soil* **408**: 369–384.
- 472 **Martens SN, Boyd RS. 1994.** The ecological significance of nickel hyperaccumulation: a plant
473 chemical defense. *Oecologia* **98**: 379–384.
- 474 **Migaszewski ZM, Galuszka A. 2015.** The characteristics, occurrence, and geochemical behavior of
475 rare earth elements in the environment: a review. *Critical Reviews in Environmental Science*
476 *and Technology* **45**: 429–471.
- 477 **Nieboer E, Richardson HS. 1980.** The replacement of the nondescript term ‘heavy metals’ by a
478 biologically and chemically significant classification of metal ions. *Environmental Pollution*
479 *series B* **1**: 3–26.
- 480 **Pletnev IV, Zernov VV. 2002.** Classification of metal ions according to their complexing properties:
481 a data-driven approach. *Analytica Chimica Acta* **455**: 131–142.
- 482 **Redling K. 2006.** Rare earth elements in agriculture with emphasis on animal husbandry. *Ludwig-*
483 *Maximilians-Universität München*.
- 484 **Reeves RD, Baker AJM, Jaffré T, Erskine PD, Echevarria G, van der Ent A. 2017.** A global
485 database for hyperaccumulator plants of metal and metalloid trace elements. *New Phytologist*
486 **218**: 407–411.

- 487 **Reeves RD, van der Ent A, Baker AJM. 2018.** Agromining: farming for metals. In Global
488 distribution and ecology of hyperaccumulator plants; van der Ent A, Echevarria G, Baker AJM,
489 Morel JL, eds, *Mineral Resource Reviews series, Cham: Springer International Publishing* pp.
490 75–92.
- 491 **Reeves RD. 2003.** Tropical hyperaccumulators of metals and their potential for phytoextraction.
492 *Plant and Soil* **249**: 57–65.
- 493 **Ruíz-Herrera LF, Sánchez-Calderón L, Herrera-Estrella L, López-Bucio J. 2012.** Rare earth
494 elements lanthanum and gadolinium induce phosphate-deficiency responses in *Arabidopsis*
495 *thaliana*, seedlings. *Plant and Soil* **353**: 231–247.
- 496 **Russell AE, Raich JW, Vitousek PM. 1998.** The ecology of the climbing fern *Dicranopteris*
497 *linearis*, on windward Mauna Loa, Hawaii. *Journal of Ecology* **86**: 765–779.
- 498 **Ryan CG, Achterbergh EV, Jamieson DN. 2005.** Advances in dynamic analysis, PIXE imaging:
499 correction for spatial variation of pile-up components. *Nuclear Instruments and Methods in*
500 *Physics Research Section B* **231**: 162–169.
- 501 **Ryan CG, Cousens DR, Sie SH, Griffin WL, Suter GF, Clayton E. 1990.** Quantitative PIXE
502 microanalysis of geological material using CSIRO proton microprobe. *Nuclear Instruments and*
503 *Methods in Physics Research Section B* **47**: 55–71.
- 504 **Ryan CG, Jamieson DN. 1993.** Dynamic analysis: on-line quantitative PIXE microanalysis and its
505 use in overlap-resolved elemental mapping. *Nuclear Instruments and Methods in Physics*
506 *Research Section B* **77**: 203–214.
- 507 **Ryan CG, Kirkham R, Hough RM, Moorhead G, Siddons DP, de Jonge MD, Paterson DJ, de**
508 **Geronimo G, Howard DL, Cleverley JS. 2010.** Elemental X-ray imaging using the Maia
509 detector array: the benefits and challenges of large solid-angle. *Nuclear Instruments and*
510 *Methods in Physics Research Section A* **619**: 37–43.

- 511 **Ryan CG, Siddons DP, Kirkham R, Li ZY, de Jonge MD, Paterson DJ, Kuczewski A, Howard**
512 **DL, Dunn PA, Falkenberg G, Boesenberg U, de Geronimo G, Fisher LA, Halfpenny A,**
513 **Lintern MJ, Lombi E, Dyl KA, Jensen M, Moorhead GF, Cleverley JS, Hough RM, Godel**
514 **B, Barnes SJ, James SA, Spiers KM, Alfeld M, Wellenreuther G, Vukmanovic Z, Borg S.**
515 **2014.** Maia X-ray fluorescence imaging: Capturing detail in complex natural samples. *Journal*
516 *of Physics: Conference Series* **499**: 012002.
- 517 **Ryan CG. 2000.** Quantitative trace element imaging using PIXE and the nuclear microprobe.
518 *International Journal of Imaging Systems and Technology* **11**: 219–230.
- 519 **Scheckel KG, Hamon R, Jassongne L, Rivers M, Lombi E. 2007.** Synchrotron x-ray absorption-
520 edge computed microtopgraphy imaging of thallium compartmentalization in *Iberis intermedia*.
521 *Plant and Soil* **294**: 305–306.
- 522 **Shan XQ, Wang HO, Zhang SZ, Zhou HF, Zheng Y, Yu H, Wen B. 2003.** Accumulation and
523 uptake of light rare earth elements in a hyperaccumulator *Dicroptheris dichotoma*. *Plant Science*
524 **165**: 1343–1353.
- 525 **Shao JF, Yamaji N, Shen RF, Ma JF. 2017.** The key to Mn homeostasis in plants: regulation of
526 Mn transporters. *Trends in Plant Science* **22**: 215–224.
- 527 **Sharma SS, Dietz K, Mimura T. 2016.** Vacuolar compartmentalization as indispensable component
528 of heavy metal detoxification in plants. *Plant, Cell & Environment* **39**: 1112–1126.
- 529 **Siddons DP, Kirkham R, Ryan CG, de Geronimo G, Dragone A, Kuczewski AJ, Li ZY, Carini**
530 **GA, Pinelli D, Beuttenmuller R, Elliott D, Pfeffer M, Tyson TA, Moorhead GF, Dunn PA.**
531 **2014.** Maia X-ray microprobe detector array system. *Journal of Physics: Conference Series* **499**:
532 012001.
- 533 **Tappero R, Peltier E, Gräfe M, Heidel K, Ginder-Vogel M, Livi KJT, Rivers ML, Marcus MA,**
534 **Chaney RL, Sparks DL. 2007.** Hyperaccumulator *Alyssum murale* relies on a different metal
535 storage mechanism for cobalt than for nickel. *New Phytologist* **175**: 641–654.

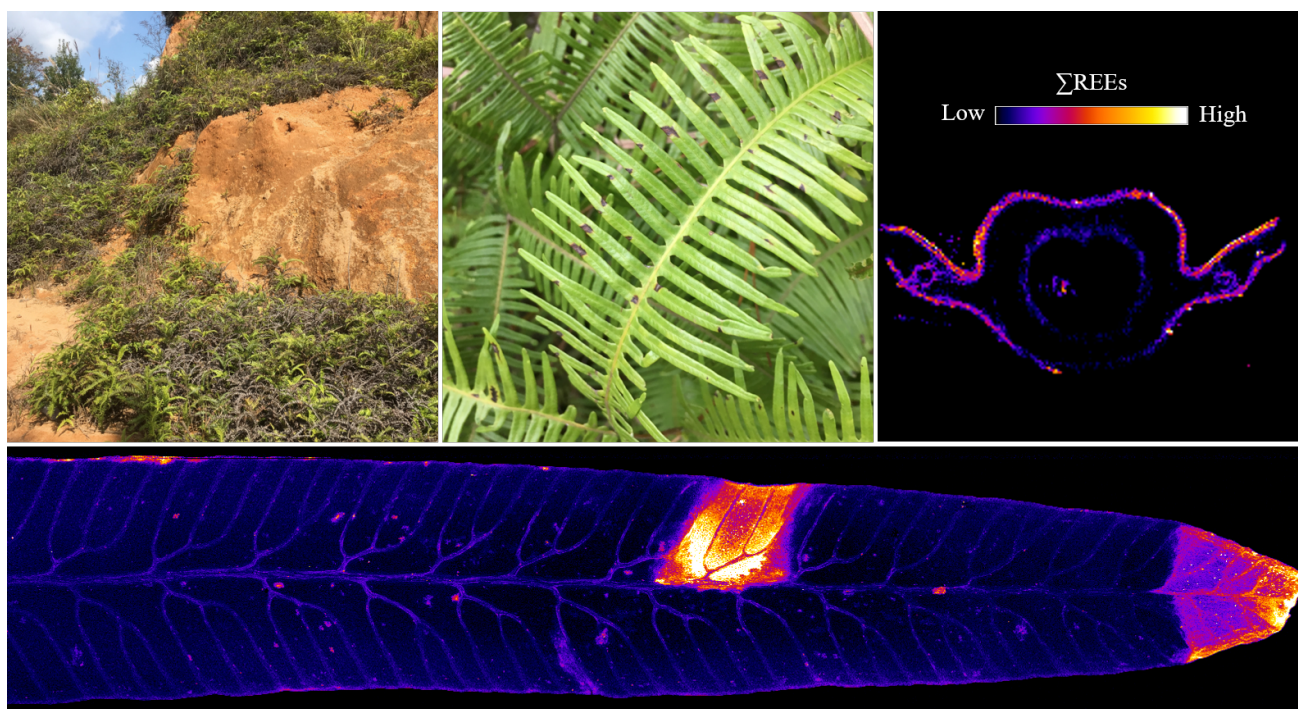
- 536 **Thomas PJ, Carpenter D, Boutin C, Allison JE. 2014.** Rare earth elements (REEs): effects on
537 germination and growth of selected crop and native plant species. *Chemosphere* **96**: 57–66.
- 538 **Tian SK, Lu LL, Yang XE, Labavitch JM, Huang YY, Brown P. 2009.** Stem and leaf
539 sequestration of zinc at the cellular level in the hyperaccumulator *Sedum alfredii*. *New*
540 *Phytologist* **182**: 116–126.
- 541 **USDA. 2018.** Agricultural Research Service, National Plant Germplasm System Germplasm
542 Resources Information Network (GRIN-Taxonomy).
- 543 **van der Ent A, Baker, AJM, Reeves RD, Pollard AJ, Schat H. 2013.** Hyperaccumulators of metal
544 and metalloid trace elements: facts and fiction. *Plant and Soil* **362**: 319–334.
- 545 **van der Ent A, Baker AJM, Reeves RD, Chaney RL, Anderson CWN, Meech JA, Erskine PD,**
546 **Simonnot MO, Vaughan J, Morel JL, Echevarria G, Fogliani B, Qiu QL, Mulligan DR.**
547 **2015.** Agromining: farming for metals in the future? *Environmental Science & Technology* **49**:
548 4773–4780.
- 549 **van der Ent A, Mulligan D. 2015.** Multi-element concentrations in plant parts and fluids of
550 Malaysian nickel hyperaccumulator plants and some economic and ecological considerations.
551 *Journal of Chemical Ecology* **41**: 396–408.
- 552 **van der Ent A, Przybyłowicz WJ, de Jonge MD, Harris HH, Ryan CG, Tylko G, Paterson DJ,**
553 **Barnabas AD, Kopittke PM, Mesjasz-Przybyłowicz J. 2018.** X - ray elemental mapping
554 techniques for elucidating the ecophysiology of hyperaccumulator plants. *New Phytologist* **218**:
555 432–452.
- 556 **Vogel-Mikuš K, Regvar M, Mesjasz-Przybyłowicz J, Przybyłowicz WJ, Simčič J, Pelicon P,**
557 **Budnar M. 2008.** Spatial distribution of cadmium in leaves of metal hyperaccumulating
558 *Thlaspi praecox* using micro-PIXE. *New Phytologist* **179**: 712–721.

- 559 **Wan SZ, Zhang CL, Chen YQ, Zhao J, Wang XL, Wu JP, Zhou LX, Lin YB, Liu ZF, Fu SL.**
560 **2014.** The understory fern *Dicranopteris dichotoma* facilitates the overstory eucalyptus trees in
561 subtropical plantations. *Ecosphere* **5**: 1–12.
- 562 **Wang H, Shan XQ, Zhang S, Wen B. 2003.** Preliminary characterization of a light-rare-earth-
563 element-binding peptide of a natural perennial fern *Dicranopteris dichotoma*. *Analytical and*
564 *Bioanalytical Chemistry* **376**: 49–52.
- 565 **Wang LH, Li JG, Zhou Q, Yang GM, Ding XL, Li XD, Cai CX, Zhang Z, Wei HY, Lu TH,**
566 **Deng XW, Huang XH. 2014.** Rare earth elements activate endocytosis in plant cells.
567 *Proceedings of the National Academy of Sciences of the United States of America* **111**: 12936–
568 12941.
- 569 **Wei ZG, Hong FS, Yin M, Li HX, Hu F, Zhao GW, Wong JWC. 2004.** Off-line separation and
570 determination of rare earth elements associated with chloroplast pigments of hyperaccumulator
571 *Dicranopteris dichotoma* by normal-phase liquid chromatography and ICP-MS. *Analytical and*
572 *Bioanalytical Chemistry* **380**: 677–682.
- 573 **Wei ZG, Hong FS, Yin M, Li HX, Hu F, Zhao GW, Wong WJ. 2005.** Subcellular and molecular
574 localization of rare earth elements and structural characterization of yttrium bound chlorophyll
575 a in naturally grown fern *Dicranopteris dichotoma*. *Microchemical Journal* **80**: 1–8.
- 576 **Wei ZG, Yin M, Zhang X, Hong FS, Li B, Zhao GW, Yan CH. 2001.** Rare earth elements in
577 naturally grown fern *Dicranopteris linearis* in relation to their variation in soils in South-
578 Jiangxi region (Southern China). *Environmental Pollution* **114**: 345–355.
- 579 **Wei ZG, Zhang HJ, Li HX, Hu F. 2006.** Research trends on rare earth element hyperaccumulator.
580 *Journal of the Chinese Rare Earth Society* **24**: 1–11. (in Chinese)
- 581 **Zhao FJ, Moore KL, Lombi E, Zhu YG. 2014.** Imaging element distribution and speciation in
582 plant cells. *Trends in Plant Science* **19**: 183–192.

- 583 **Zhao GW, Hong FS, Wei ZG, Gu YH, Hu TD, Xie YN, Liu T, Tao Y. 1999.** Light rare earth
584 element speciation of chlorophyll a in naturally grown fern *Dicranopteris linearis* by EXAFS.
585 *Progress in Natural Science* **9**: 1133–1135.
- 586 **Zhao J, Wan SZ, Li ZA, Shao YH, Xu GL, Liu ZF, Zhou LX, Fu SL. 2012.** *Dicranopteris*-
587 dominated understory as major driver of intensive forest ecosystem in humid subtropical and
588 tropical region. *Soil Biology and Biochemistry* **49**: 78–87.

589 GRAPHICAL ABSTRACT

590



591

592

593

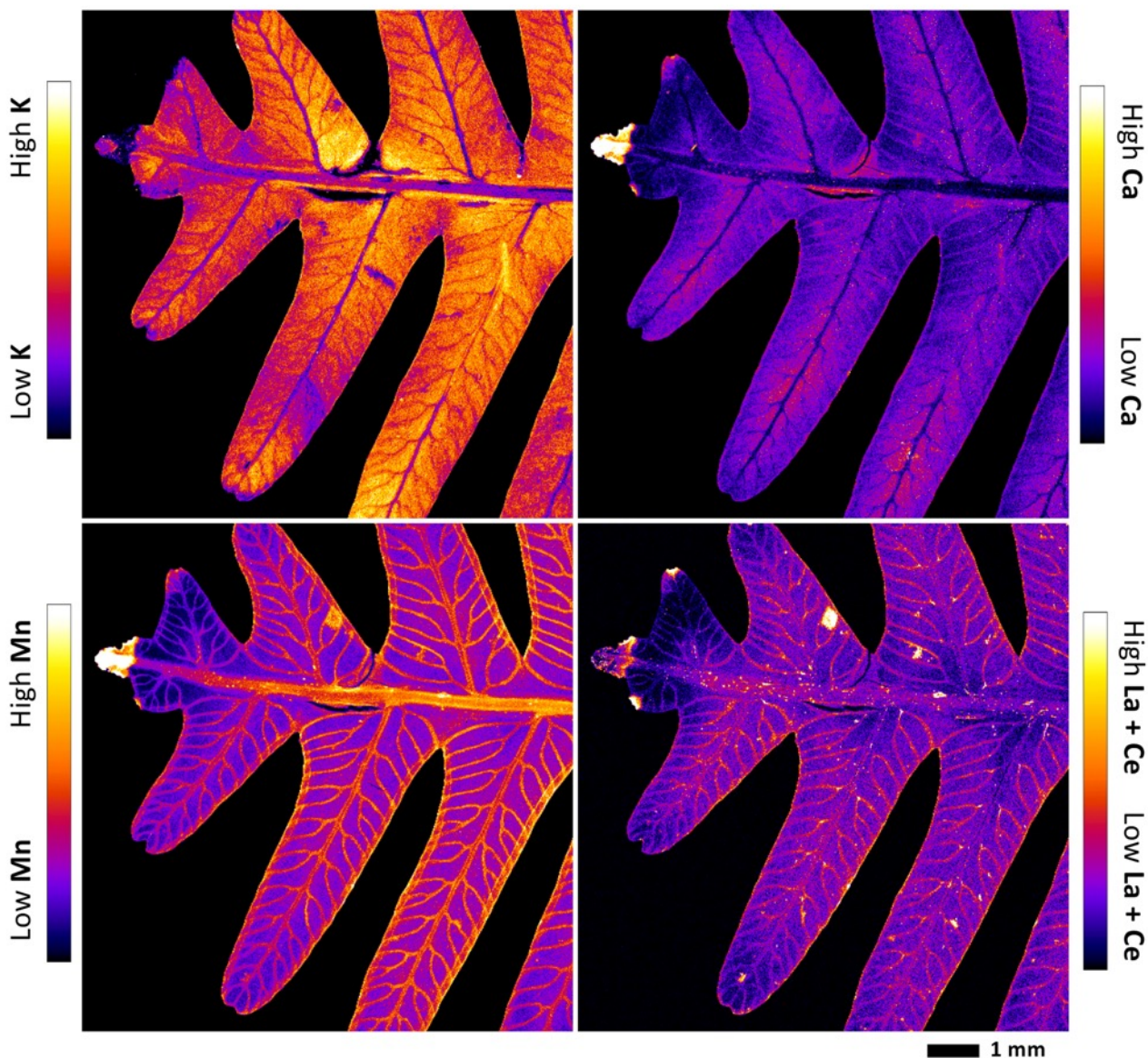


594

595

596 **Fig. 1.** Live *Dicranopteris linearis* grown at (a) the understory of *Cunninghamia lanceolata*; (b) an
597 ion-adsorption REE mine tailing abandoned for about 10 years at Ganzhou, Jiangxi Province,
598 Southern China.

599

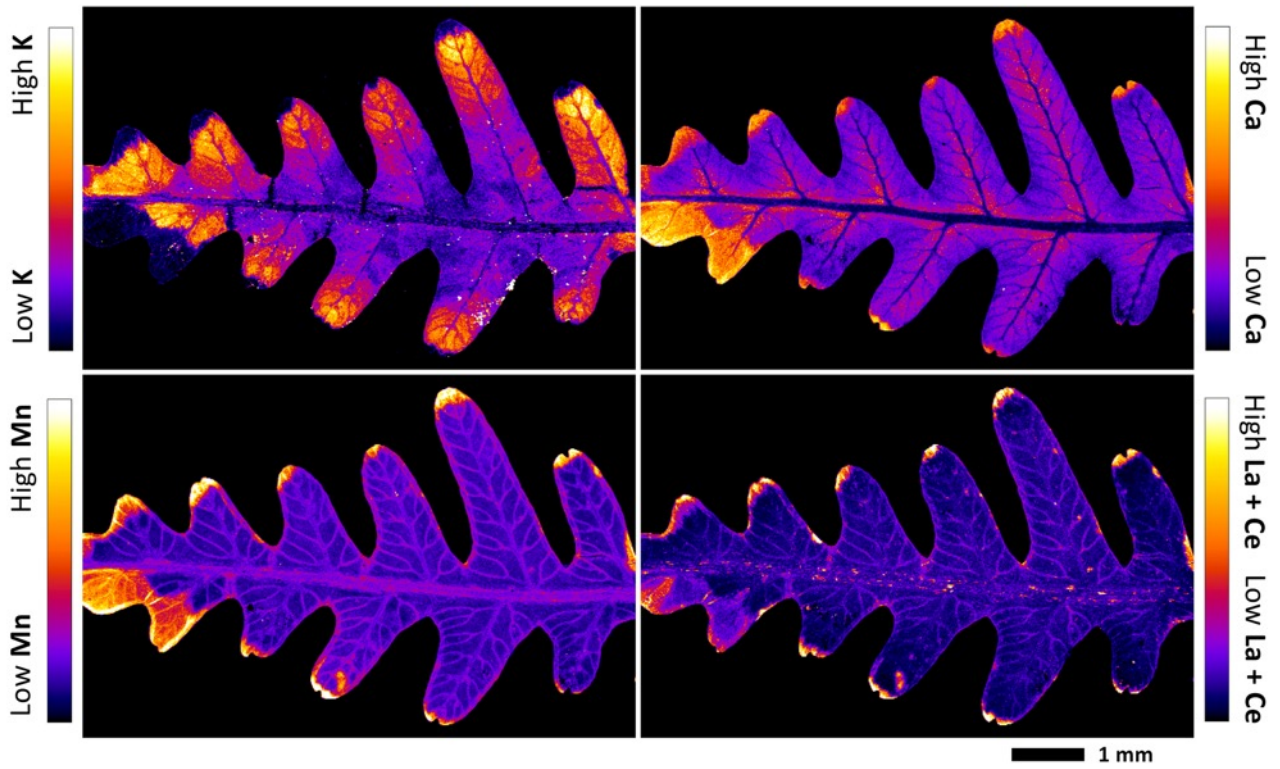


600

601

602 **Fig. 2.** Elemental μ -XRF maps of fresh *Dicranopteris linearis* pinna. The maps measure 8.86×8.56
 603 mm. The elemental image was acquired in step size $15 \mu\text{m}$ with dwell 15 ms per pixel, 12.0 keV,
 604 incident beam.

605

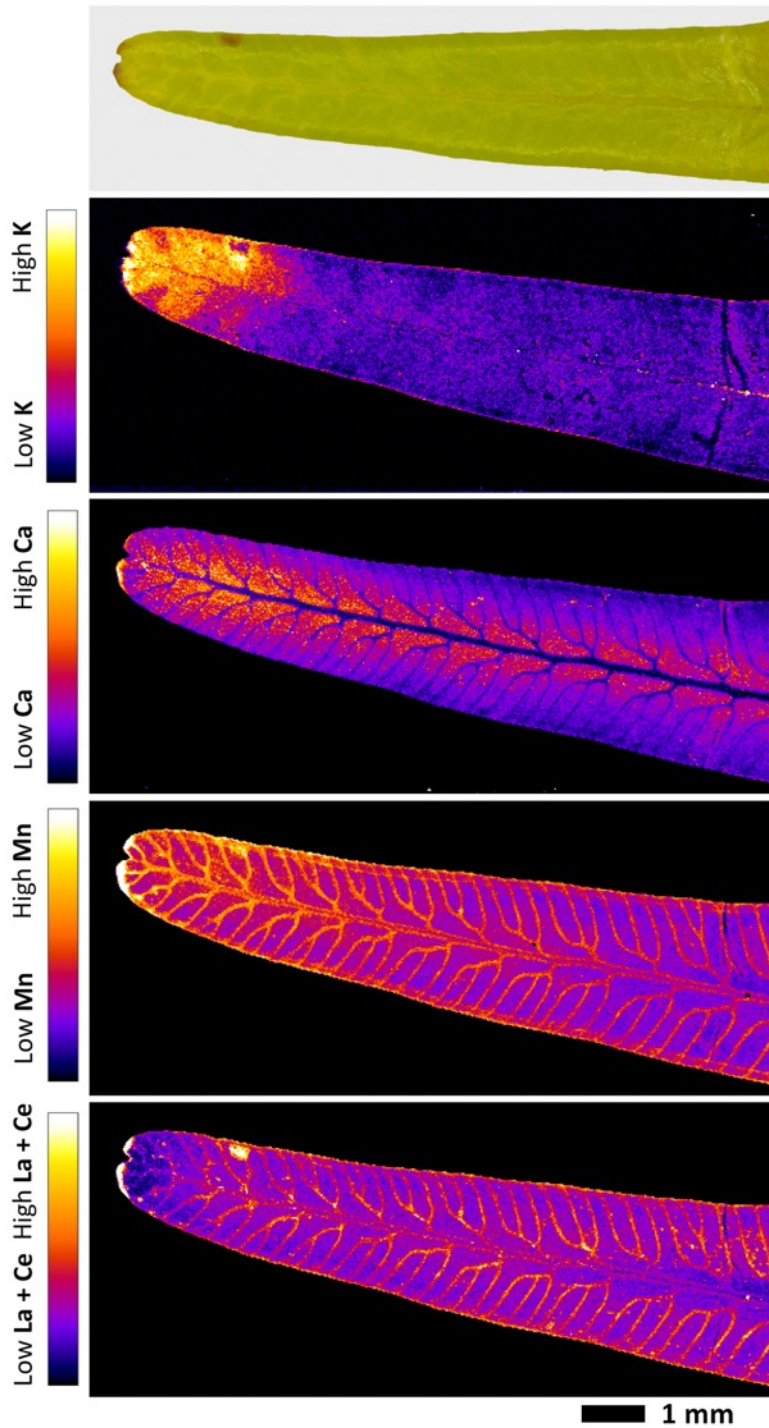


606

607

608 **Fig. 3.** Elemental μ -XRF maps of fresh *Dicranopteris linearis* pinna. The maps measure 13.1×8.58
 609 mm. The elemental image was acquired in step size $25 \mu\text{m}$ with dwell 15 ms per pixel, 12.0 keV,
 610 incident beam.

611

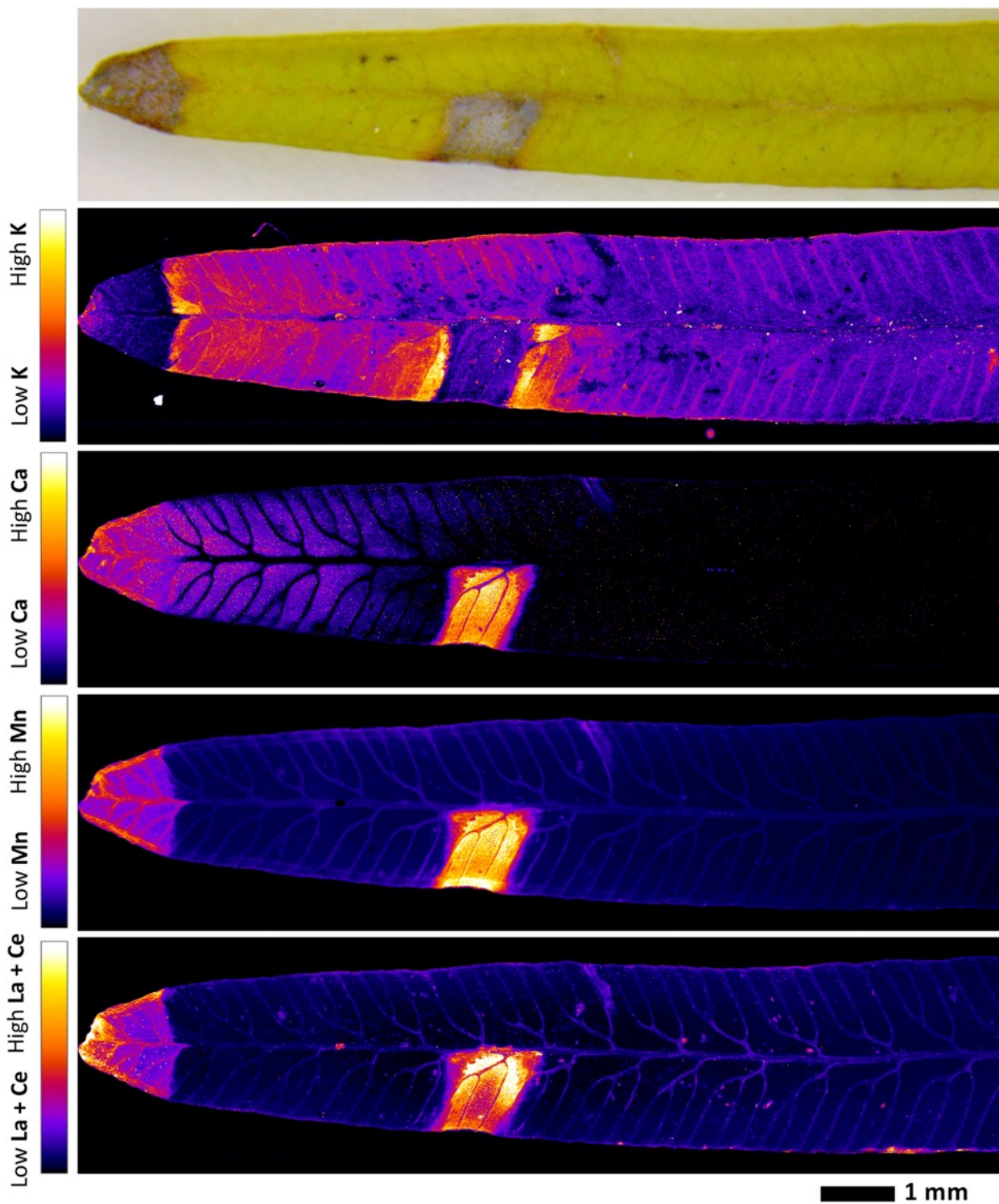


612

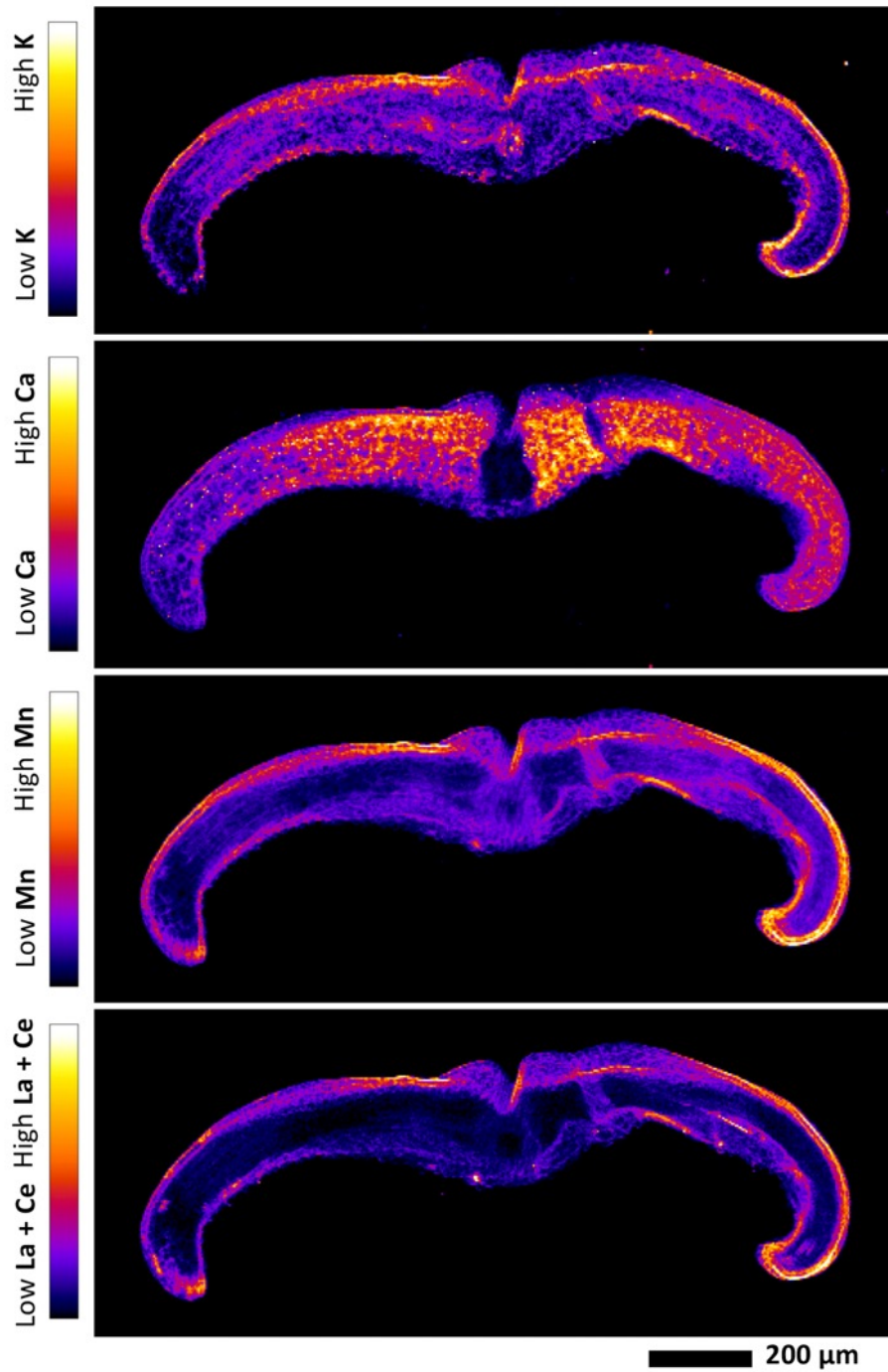
613

614 **Fig. 4.** Elemental μ -XRF maps of fresh *Dicranopteris linearis* pinnule. The maps measure 10.2 ×
 615 4.26 mm. The elemental image was acquired in step size 20 μ m with dwell 20 ms per pixel, 12.0
 616 keV, incident beam.

617



618
 619 **Fig. 5.** Elemental μ -XRF maps of fresh *Dicranopteris linearis* pinnule. The maps measure $12.95 \times$
 620 2.88 mm. The elemental image was acquired in step size $8 \mu\text{m}$ with dwell 15 ms per pixel, 12.0 keV,
 621 incident beam.

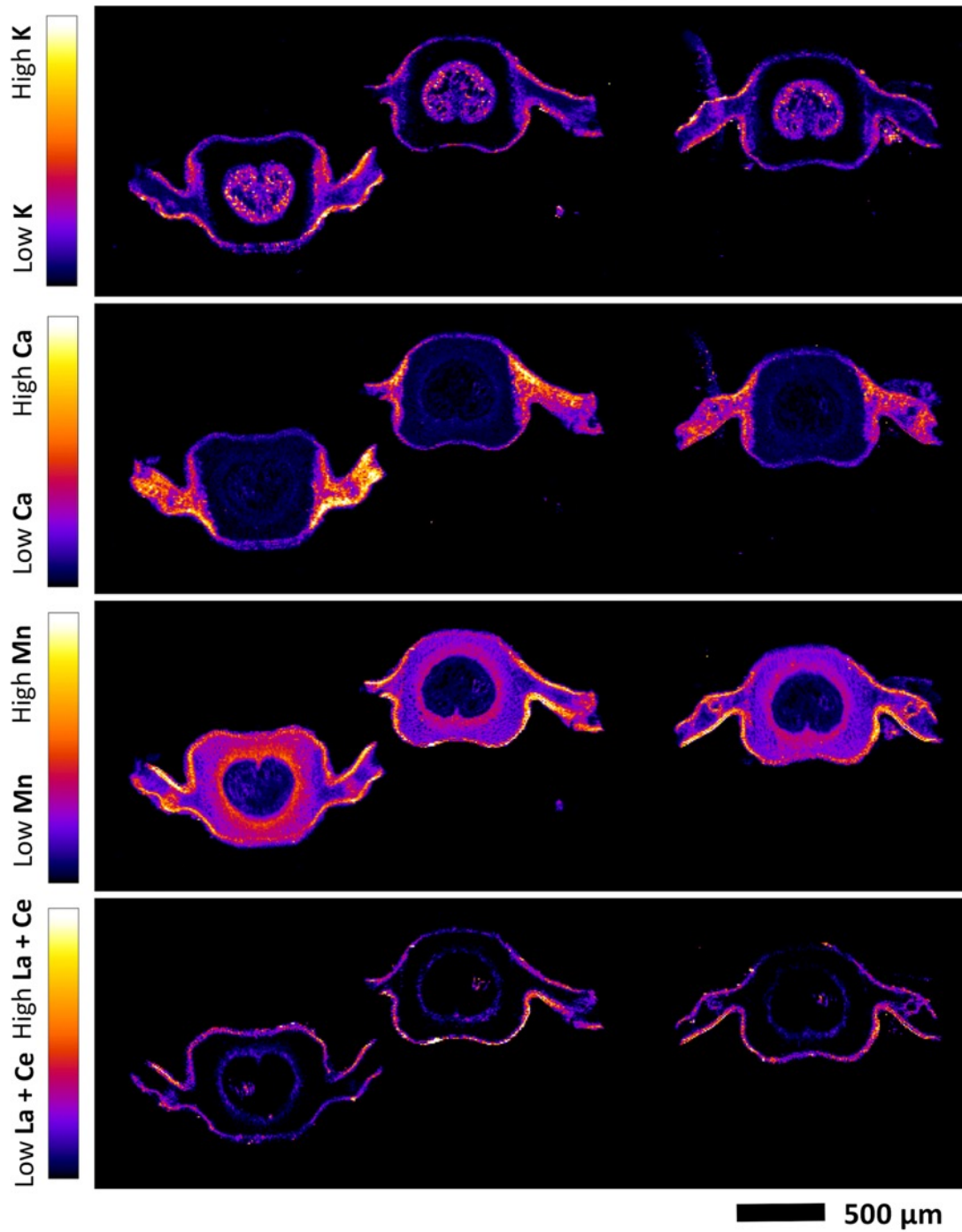


622

623

624 **Fig. 6.** Elemental μ -XRF maps of fresh *Dicranopteris linearis* pinnule cross-section. The maps
 625 measure 2.25×0.86 mm. The elemental image was acquired in step size $5 \mu\text{m}$ with dwell 15 ms per
 626 pixel, 12.0 keV, incident beam.

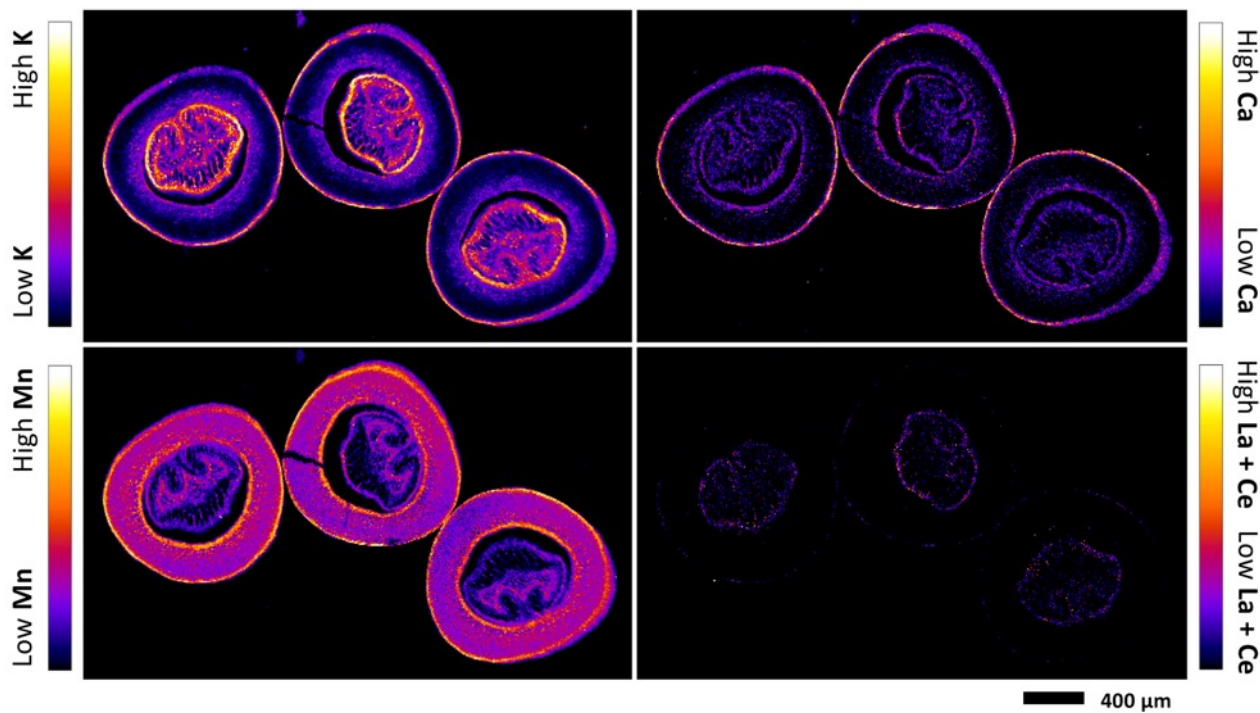
627



628

629

630 **Fig. 7.** Elemental μ -XRF maps of fresh *Dicranopteris linearis* midvein cross-section of pinna. The
 631 maps measure 4.70×1.57 mm. The elemental image was acquired in step size $8 \mu\text{m}$ with dwell 15
 632 ms per pixel, 12.0 keV, incident beam. The concave side represents the adaxial side in the figure.



633

634 **Fig. 8.** Elemental μ -XRF maps of fresh *Dicranopteris linearis* petiole cross-section of pinna. The

635 maps measure 5.62 x 3.41 mm. The elemental image was acquired in step size 12 μ m with dwell 15

636 ms per pixel, 12.0 keV, incident beam.

637 TABLES

638

639 **Table 1.** Bulk elemental concentrations in pinna of *Dicranopteris linearis* (mg kg⁻¹ dry weight).

640

Type	n	Al	Si	REEs*	Ca	Mn	P	K
Live pinna	1	2860	13400	1540	1330	1350	232	3330
	2	3180	19500	2450	2160	1340	179	2600
	3	1490	11800	1400	1160	1020	213	3390
	4	3860	14100	2190	2580	2230	220	2700
Mean ± sd		2850±997a	14700±3310a	1900±505a	1810±676a	1480±523b	211±23.0b	3000±413b
Standing litter pinna	1	4910	36600	3620	2300	541	130	240
	2	5280	36800	3750	988	241	156	432
	3	4370	28200	3130	908	149	100	131
Mean ± sd		4850±455b	33900±4910b	3500±327b	1400±779a	310±205a	129±28.0a	268±152a

641 * The summed concentration of La, Ce, Pr, Nd, Sm, Eu, Gd, Tb, Dy, Ho, Er, Tm, Yb, Lu and Y, see the concentration of each rare earth element
642 in *Table S2*.

Supporting Information

Spatially-resolved localization of lanthanum and cerium in the rare earth element hyperaccumulator fern *Dicranopteris linearis* from China

Wen-Shen Liu^{1,2,3}, Antony van der Ent^{4,5}, Peter D. Erskine⁴, Jean Louis Morel⁵, Guillaume Echevarria^{4,5}, Kathryn M. Spiers⁶, Emmanuelle Montargès-Pelletier⁷, Rong-Liang Qiu^{1,2,3}, Ye-Tao Tang^{1,2,3,*}

¹School of Environmental Science and Engineering, Sun Yat-sen University, Guangzhou 510275, China.

²Guangdong Provincial Key Laboratory of Environmental Pollution Control and Remediation Technology, Sun Yat-sen University, Guangzhou 510275, China.

³Guangdong Provincial Engineering Research Center for Heavy Metal Contaminated Soil Remediation, Sun Yat-sen University, Guangzhou 510275, China.

⁴Centre for Mined Land Rehabilitation, Sustainable Minerals Institute, The University of Queensland, St Lucia, Queensland 4072, Australia.

⁵Université de Lorraine, INRA, Laboratoire Sols et Environnement, Nancy 54000, France.

⁶Photon Science, Deutsches Elektronen-Synchrotron DESY, Hamburg 22607, Germany.

⁷CNRS – Université de Lorraine Laboratoire Interdisciplinaire des Environnements Continentaux, Vandoeuvre-lès-Nancy F-54500, France.



28

29

30 **Fig. S1.** Live *Dicranopteris linearis* grown at (a) the understory of *Cunninghamia lanceolata*; (b) an
31 ion-adsorption REE mine tailing abandoned for about 10 years at Ganzhou, Jiangxi Province,
32 Southern China.

33



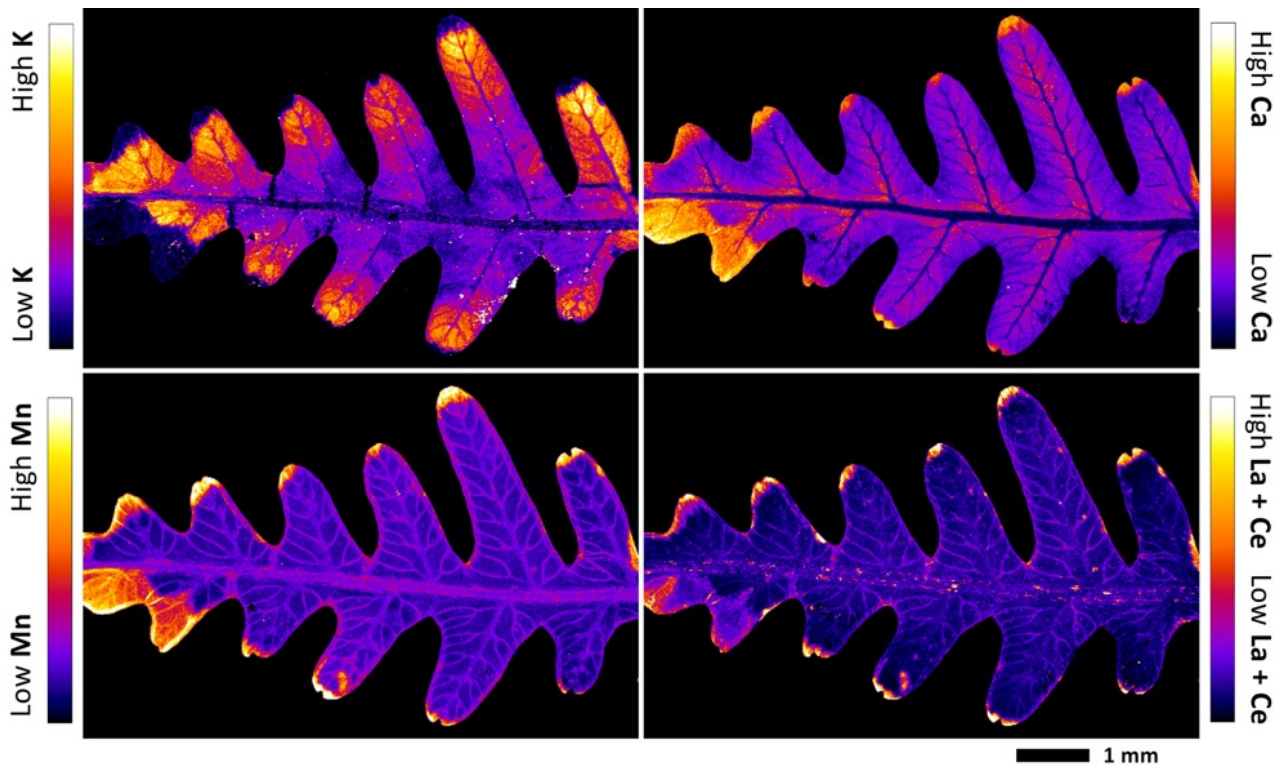
34

35

36 **Fig. S2.** *Dicranopteris linearis* growing at an ion-adsorption REE mine tailings. (a) *D. linearis*

37 thicket with both live pinnae and dead standing litter pinnae; (b) dead standing litter pinnae; (c)

38 morphological characteristics of *D. linearis*.



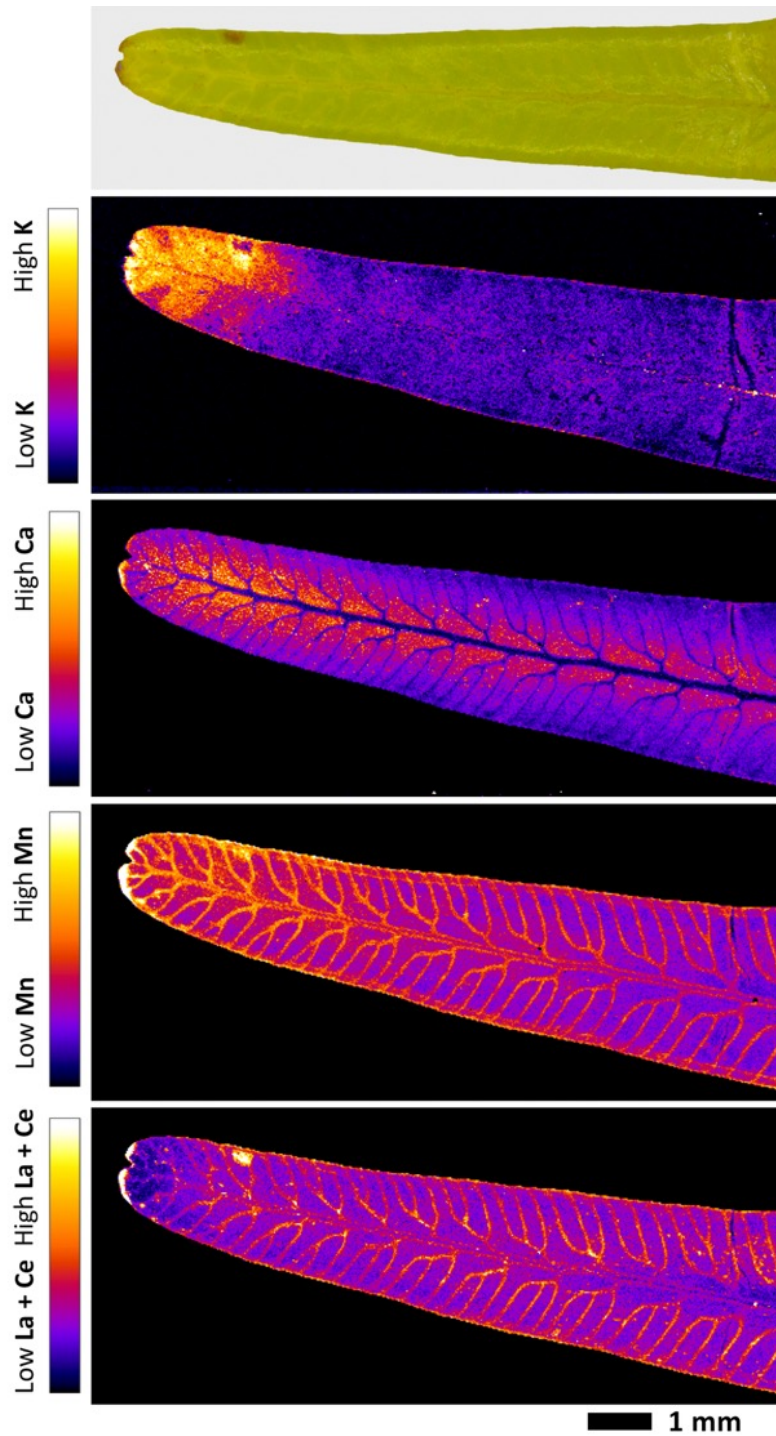
39

40

41 **Fig. S3.** Elemental μ -XFM maps of hydrated *Dicranopteris linearis* pinna. The maps measure $13.1 \times$

42 8.58 mm. The elemental image was acquired in step size $25 \mu\text{m}$ with dwell 15 ms per pixel, 12.0

43 keV, incident beam.

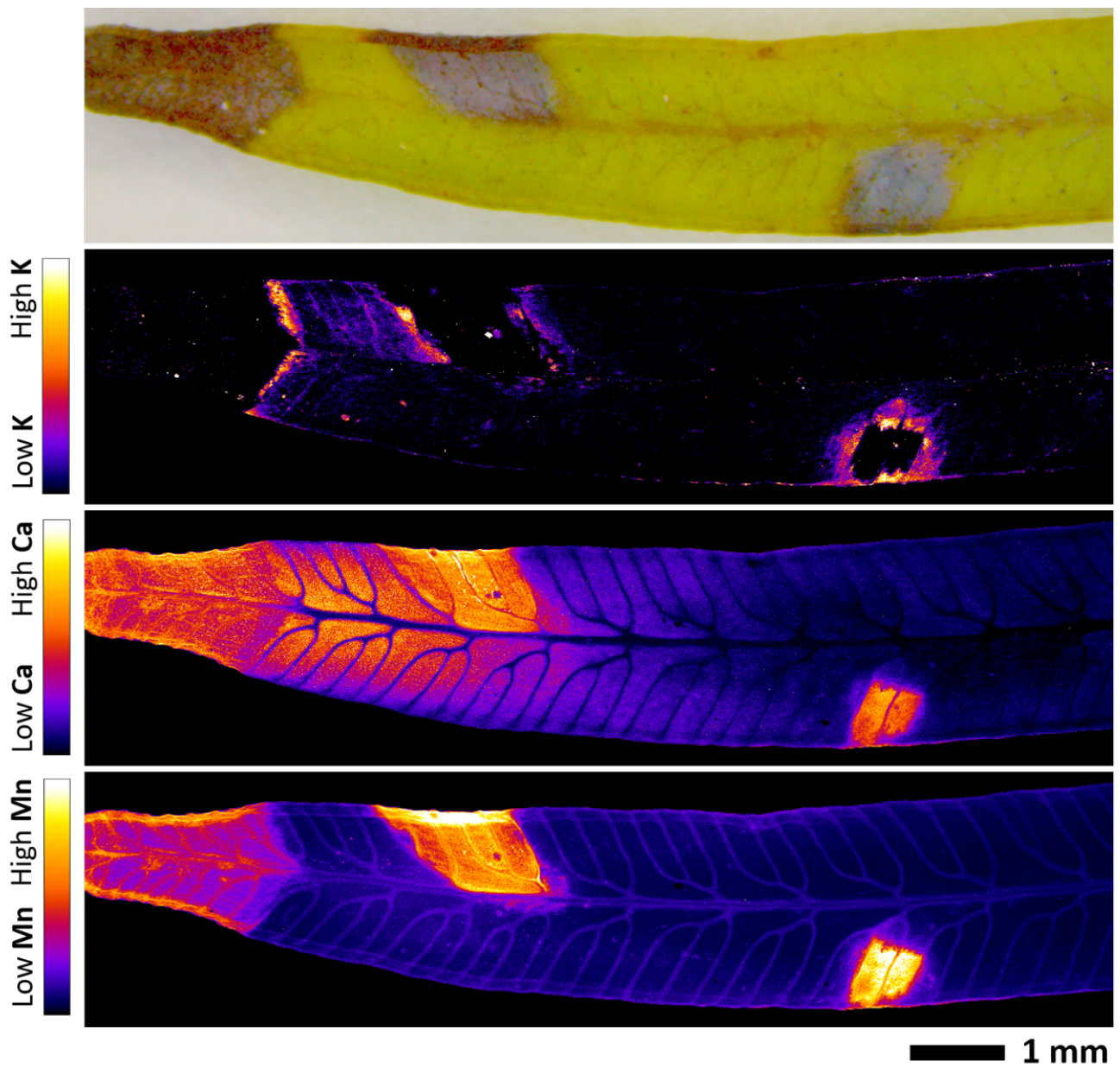


44

45

46 **Fig. S4.** Elemental μ -XFM maps of hydrated *Dicranopteris linearis* pinnule. The maps measure 10.2
 47 \times 4.26 mm. The elemental image was acquired in step size 20 μ m with dwell 20 ms per pixel, 12.0
 48 keV, incident beam.

49



50

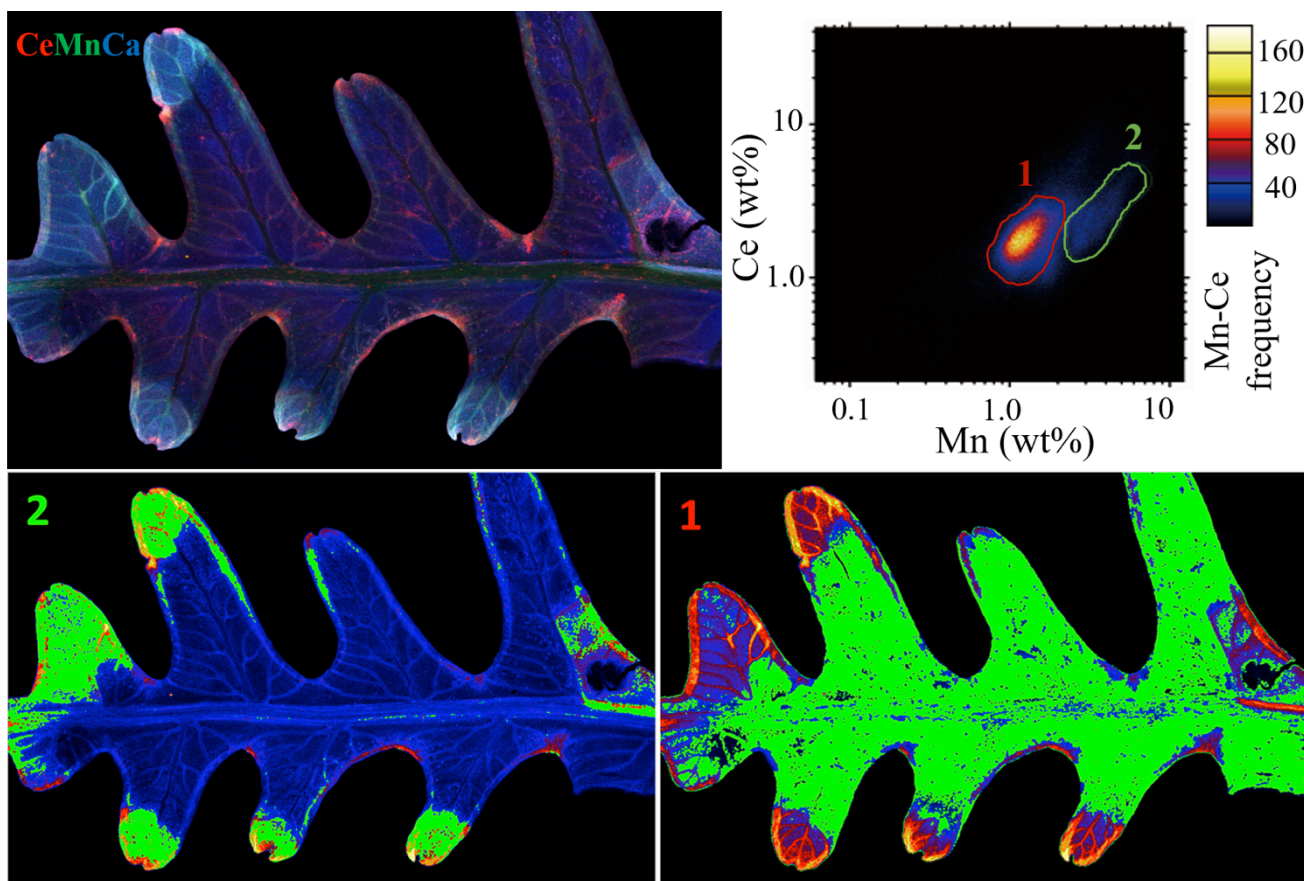
51

52 **Fig. S5.** Elemental μ -XRF maps of hydrated *Dicranopteris linearis* pinnule. The maps measure

53 11.25×2.79 mm. The elemental image was acquired in step size $8 \mu\text{m}$ with dwell 15 ms per pixel,

54 12.0 keV, incident beam. The REE content was below detection limits.

55

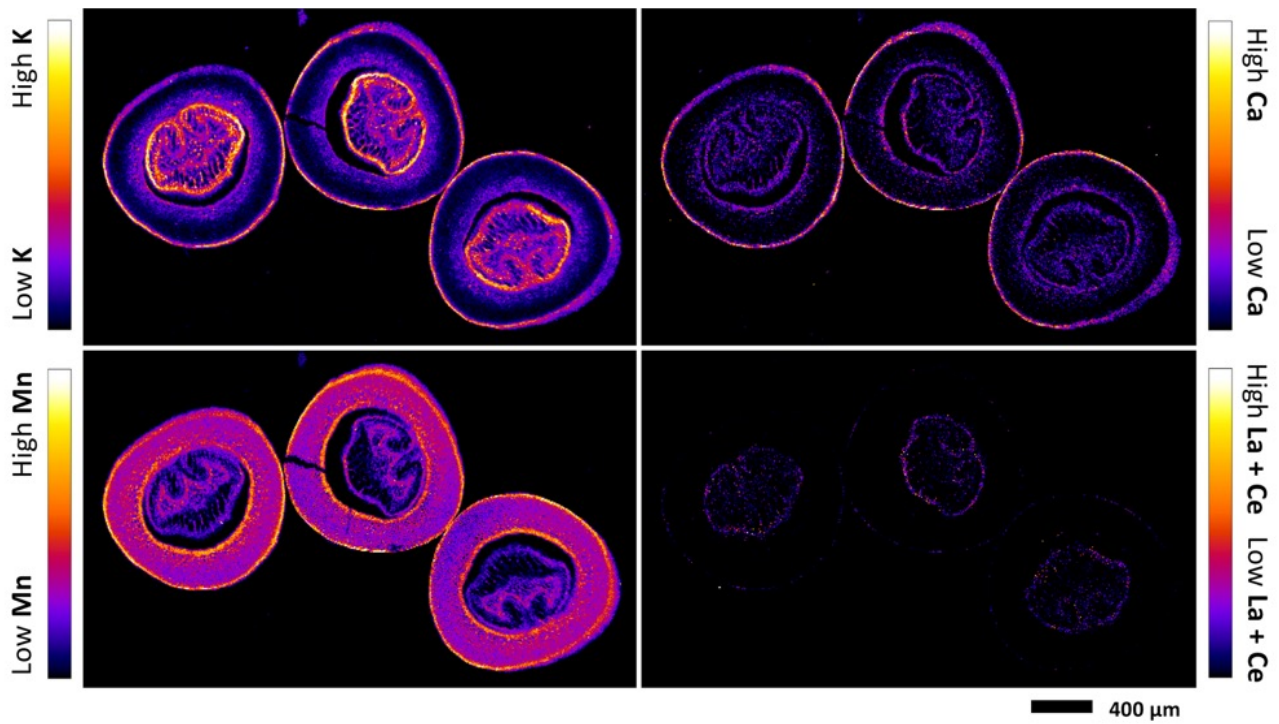


56

57

58 **Fig. S6.** Tri-color elemental maps (red = Ce, green = Mn, blue = Ca) in a pinna (top left) and element
59 association (Ce and Mn) frequency plots (top right). Two areas were marked and plotted on the pinna
60 elemental map (bottom two panels) showing occurrence of Mn-Ce associations in green.

61



62

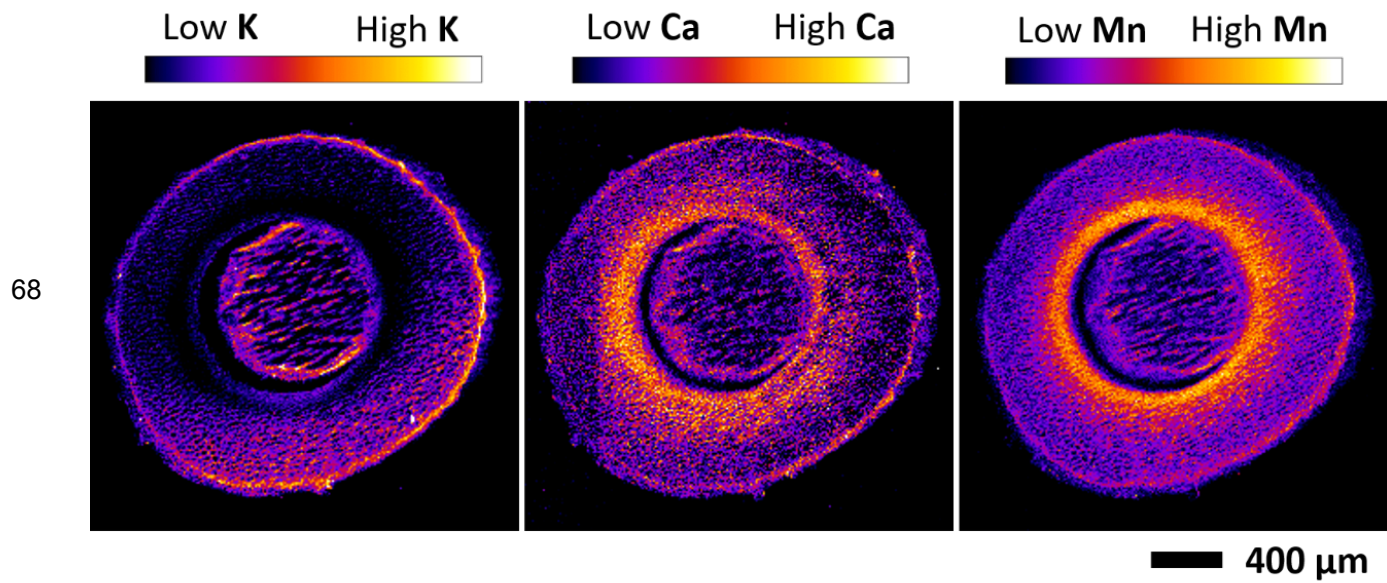
63

64 **Fig. S7.** Elemental μ -XFM maps of hydrated *Dicranopteris linearis* petiole cross-section of pinna.

65 The maps measure 5.62 x 3.41 mm. The elemental image was acquired in step size 12 μ m with dwell

66 15 ms per pixel, 12.0 keV, incident beam.

67



69

70 **Fig. S8.** Elemental μ -XRF maps of hydrated *Dicranopteris linearis* stolon cross-section. The maps
71 measure 2.84 x 2.81 mm. The images were acquired in step size 12 μm with dwell 15 ms per pixel,
72 12.0 keV, incident beam. The REE content was below detection limits.

73 **Table S1.** Rare earth elements concentrations in *Dicranopteris linearis* and rhizosphere soil

74 collected from different sites.

75

Type	Aboveground part / mg kg ⁻¹	Underground part / mg kg ⁻¹	Rhizosphere soil / mg kg ⁻¹	Aboveground part / Rhizosphere soil	Aboveground part / Underground part
MT	1470±199 a	727±426 a	518±208 a	3.27±1.55 a	2.77±1.89 a
TE	875±449 ab	198±66.0 bc	304±159 ab	4.09±3.57 a	5.12±3.49 a
NM	1430±733 a	393±71.8 b	573±307 a	2.92±1.45 a	3.52±1.18 a
HB	1160±806 ab	189±93.3 bc	363±81.9 ab	3.21±1.88 a	8.01±6.94 a
LB	297±296 b	24.8±18.2 d	117±52.6 b	2.68±2.32 a	18.4±22.1 a

76

77 *Dicranopteris linearis* samples and rhizosphere soils were collected in non-mining area near ion-adsorption REE

78 mine tailings (NM), ion-adsorption REE mine tailings (MT), edge of the ion-adsorption REE mine tailings (TE),

79 high levels of REEs background (HB) from Ganzhou, Jiangxi province, and low levels of REEs background (LB)

80 from Guangzhou, Guangdong province of China. Different letters in the figure represent significant difference

81 among each group (ANOVA, Duncan, $p < 0.05$). Plant samples were divided into aboveground part and

82 underground part, thoroughly washed with deionized water, dried in an oven at 105 °C for 1 hour and then 60 °C for

83 48 hours, and then carefully crushed. Soil samples were air-dried and sieved to 0.15 mm. 50 ± 0.5 mg of dry plant

84 samples and soil samples were introduced in a Teflon crucible equipped with cylinder sleeve, heated to 195 °C in an

85 oven for 48 hours after adding 3 mL HNO₃ (UP, 65%) and 1 mL HF, and then evaporated on a hot plate to dryness.

86 One mL 20% HNO₃ was added to the Teflon crucible and heated to 195 °C for 2 hours (1). The digestion solution

87 was transferred to 15 mL tubes with 2% HNO₃. The REEs were determined using an X Series 2 ICP-MS (Thermo,

88 USA). The internal standard used was ¹¹⁵In. The external standard used during analysis was shrub branches and

89 leaves (GBW07602) and yellow-red soil (GBW07405). The recovery of In during the testing was 95–105%. The

90 measured values of the external standards were in the range of standard values of references.

91 **Table S2.** Rare earth elements concentrations of live pinnae and dead standing litter pinnae collected from an ion-adsorption REE mine tailing in

92 Southern China (mg kg⁻¹ dry matter).

93

Type	La	Ce	Pr	Nd	Sm	Eu	Gd	Tb	Dy	Ho	Er	Tm	Yb	Lu	Y
Living pinna (n=4)	686±2 84 a	355±2 38 a	121±30 .2 a	366±63 .2 a	82.9±6. 68 a	12.4±0. 74 a	80.0±6. 51 a	9.00±1. 16 a	37.6±8. 15 a	5.92±1. 71 a	15.2±3. 51 a	1.58±0. 55 a	8.11±3. 07 a	1.07±0. 44 a	114±29 .2 a
Dead standing pinna (n=3)	1710± 420 b	277±1 10 a	325±63 .0 b	948±16 1 b	229±63. 9 b	35.1±8. 86 b	188±39. 1 b	21.7±5. 42 b	85.2±22 .0 b	12.7±3. 39 b	33.3±8. 81 b	3.25±0. 97 b	17.2±5. 56 b	2.28±0. 76 b	236±60 .0 b

94 *Different letters in the figure represent significant difference among each group (ANOVA, Duncan, p<0.05).*

95 **Table S3** Rare earth elements concentrations in the shoot of accumulator plants

96

Family ^(a)	Species	REE / mg kg ⁻¹	Sampling sites	Reference
Gleicheniaceae	<i>Dicranopteris linearis</i>	Up to 7000	China	(2)
	<i>Dicranopteris strigose</i>	12; BF>1 ^(b)	Japan	(3)
Juglandaceae	<i>Carya cathayensis</i>	2300 ^(c)	USA	(4)
	<i>Carya tomentosa</i>	136		(5)
Thelypteridaceae	<i>Pronephrium simplex</i>	1230		(1)
	<i>Pronephrium triphyllum</i>	1030		(6)
Phytolaccaceae	<i>Phytolacca americana</i>	1040	China	(7)
	<i>Blechnum orientale</i>	1020		
Blechnaceae	<i>Woodwardia japonica</i>	367		(8)
Lindsaeaceae	<i>Stenoloma chusana</i>	725		
Athyriaceae	<i>Athyrium yokoscence</i>	202		(9)
Dryopteridaceae	<i>Dryopteris erythrosora</i>	32; BF>1 ^(b)	Japan	(3)
	<i>Dryopteris fuscipes</i>	10; BF>1 ^(b)		
	<i>Asplenium filipes</i>	25; BF>1 ^(b)		
	<i>Asplenium hondoense</i>	14; BF>1 ^(b)		
Aspleniaceae	<i>Asplenium ruprechtii</i>	40; BF>1 ^(b)		
	<i>Asplenium ritoense</i>	12; BF>1 ^(b)		
	<i>Asplenium subnomale</i>	14; BF>1 ^(b)		
Blechnaceae	<i>Blechnum niponicum</i>	9.7; BF>1 ^(b)		
Adiantaceae	<i>Adiantum monochlamys</i>	11; BF>1 ^(b)		

97

98 The table is adapted from Liu et al. (10) with minor modifications. (a) The lanthanum (La)

99 concentration in *Glochidion triandrum* (Phyllanthaceae) leaf < 1 mg kg⁻¹, thus not a REEs

100 accumulator and removed from the figure; (b) means the La concentration in the shoot, BF means
101 bioaccumulation factor (i.e. La in the shoot / La in the soil); (c) the REE concentrations in the ash.

102